Multi-omics construction of prognostic and immunotherapy-related gene signature and small molecule drug prediction for skin cutaneous melanoma

Jiahua Xing
Nankai University
Ziqi Jia
Chinese Academy of Medical Sciences
Yan Li
Chinese PLA General Hospital
Yan Han (hanyanhyy10@163.com)
Chinese PLA General Hospital

Research Article

Keywords: Skin cutaneous melanoma, Tumor microenvironment, Prognostic signature, Immunotherapy, Bioinformatics

Posted Date: May 19th, 2022

DOI: https://doi.org/10.21203/rs.3.rs-1661051/v1

Abstract

Background: Skin cutaneous melanoma (SKCM), a kind of skin cancer with a high rate of advanced mortality, exhibits a wide variety of driver and transmitter gene alterations in the immunological tumor microenvironment (TME) associated with tumor cell survival and proliferation.

Methods: We analyzed the immunological infiltration of TME cells in normal and malignant tissues using 469 SKCM and 556 normal skin samples. We used a single sample gene set enrichment assay (ssGSEA) to quantify the relative abundance of 28 cells, developed a riskScore prognostic model using the LASSO COX regression model, and performed small molecule drug screening and molecular docking validation, which was finally validated using qRT-PCR and IHC.

Results: We developed a prognosis model around seven essential protective genes for the first time, dramatically elevated in tumor tissues, as did immune cell infiltration. The results of multivariate Cox regression demonstrated that riskScore is an independent and robust prognostic indicator, and its predictive usefulness in immunotherapy was verified. Additionally, we identified Gabapentin as a possible small molecule therapeutic for SKCM.

Conclusions: A riskScore model was developed in this work to analyze patient prognosis, TME cell infiltration features, and treatment responsiveness. The development of this model aid in predicting patient response to immunotherapy, but it also has significant implications for the development of novel immunotherapeutic agents and the promotion of tailored treatment regimens.

1. Introduction

The incidence of skin cutaneous melanoma (SKCM), a malignant tumor of the skin and mucous membranes, has been increasing globally over the past few decades. There were more than 100,000 cases of SKCM recorded in the United States in 2021 [1]. Although SKCM accounts for only 5% of all skin cancers, up to 80% of skin cancer deaths are associated with SKCM [2]. The incidence of SKCM is increasing by 3%-7% annually, posing a severe threat to human life and health [3]. Overall 10-year survival statistics for patients with early-stage SKCM (stages I and II) remain favorable, ranging between 75% and 94% [4]. In general, early-stage SKCM has a high cure rate after complete resection. In contrast, in patients with advanced SKCM (stages III and IV) with clinical lymph node involvement, the mortality rate is up to 70%, and the 5-year survival rate is less than 16% [5]. SKCM comprises a small proportion of all skin tumors; compared to other skin tumors, SKCM has clinical features such as high malignancy, high recurrence rate, facile metastasis, high late mortality, and high therapeutic resistance [6] [7] [8]. Although SKCM has received increasing clinical attention, its clinical efficacy and patient prognosis have not reached the expected level due to its complex genetic and molecular mechanisms [9].

The treatment and management of SKCM has changed significantly in recent years with the advent of immune checkpoint inhibitors (ICIs), which have also become the new standard of care for high-risk and metastatic SKCM [10] [11]. In a minority of SKCM patients with lasting responses, immunotherapies such

as ICIs (anti-PD-1/L1 antibodies and anti-CTLA-4 antibodies) have a favorable prognosis. However, most patients do not have a favorable prognosis from them. This disparity in clinical response rates between tumors of the same and different types suggests innate and acquired immunological resistance to immune checkpoints in tumor tissue [12] [13] [14]. Numerous researchers currently believe that the tumor microenvironment (TME) comprises a network of tumor cells and stromal cells (fibroblasts, vascular cells, and inflammatory immune cells), which play a crucial role in immune evasion and immunotherapy resistance [15]. Therefore, this study utilized immune-related gene sets in conjunction with clinical data from many databases to build a prediction model with TME immune cell infiltration features as its core, then verified it with multi-omics. In addition, for the first time, this study employs highly expressed tumor-protective genes as the core of the model and small molecule therapeutic screening and molecular docking validation.

2. Material And Method

2.1 Gene expression profiles of SKCM and normal skin tissue

We first downloaded the TCGA TARGET GTEx dataset from the UCSC database (https://xena.ucsc.edu/) and extracted the normal group in TCGA and the normal skin data in GTEx as the control group. Our study included 1025 SKCM expression profile cohorts, including the TCGA-SKCM and GTEx. We downloaded the COUNT gene expression values from public genomic data using the R package TCGAbiolinks [16]. 469 SKCM samples and 556 normal samples were obtained for this study. We utilized the R package Combat algorithm to correct for batch effects due to abiotic bias. In addition, we downloaded immune-related genes from the immport (https://www.immp ort.orgc) database for subsequent analysis.

2.2 Screening of immune-related differentially expressed genes (DEGs)

To identify key molecules associated with patients' prognosis and TME cellular immune infiltration characteristics, we identified differentially expressed genes (DEGs) in SKCM and normal skin tissue using the empirical Bayes method in the R language limma-voom package. We used $P<0.01$ and $|logFC|\geq 2$ as a cut-off criterion to screen significantly DEGs. In addition, we utilized the R package ClusterProfiler for gene ontology (GO) and Kyoto Encyclopedia of Genes and Genomes (KEGG) enrichment analysis to investigate further the potential biological processes related to immune-related DEGs [16].

2.3 Multi-omics analysis to identify key molecules

First, we submitted all DEGs to the STRING database to generate network maps of their protein-to-protein interactions (PPI). Then, we identify significant sub-network modules from the PPI network using the MCODE plugin for Cytoscape. We established the cutoff criterion as follows: degree cutoff=10, node score cutoff=0.2, k-core=2, max.depth=100. We will choose genes with high connection and significant predictive value ($P<0.01$) among significant subnetwork modules as important molecules [17]. Finally, we chose CD86, CXCL9, FCGR3A, GZMB, PRF1, STAT1, and TLR7 as our key molecules. We utilized TCGA

mutation data to show key molecules' mutation frequencies and mutation types in SKCM patients. 467 SKCM patients with complete clinical annotation were available for SKCM survival analysis. We utilized the R package survminer to determine appropriate cut-off points, categorized patients into high- and low-risk groups and employed the Human Protein Atlas (https://www.prote inatlas.org/) database to evaluate the protein expression of key molecules between SKCM and normal skin tissue.

2.4 Extrapolation of TME infiltrating cells

We utilized single sample gene set enrichment analysis (ssGSEA) to estimate the infiltration abundance of each TME cell based on the Cibersort gene set [18]. We accommodated the enrichment scores for each TME cell subtype using the ESTIMATE algorithm to control the bias caused by tumor purity [19]. We employed 28 human TME cell subtypes and expressed the abundance of each TME-infiltrating cell by the adjusted enrichment scores determined using ssGSEA.

2.5 Construction of a key molecules-based prognostic model

We constructed riskScore models based on the involvement of these seven critical genes in the course of SKCM in order to analyze the relevance of these molecules in patient prognosis, TME immune cell infiltration, and immunotherapy responsiveness. We created prognostic models for fitting the overall survival (OS) of SKCM patients using least absolute shrinkage and selection operator (LASSO) Cox regression analysis. In order to construct the optimal prognostic model, we utilized the R language's glmnet package to select and reduce the variables so that some of the regression coefficients were strictly equal to 0. In addition, we employ 10 cross-validations to establish the penalty parameter (λ) of the prognostic model and adhere to the minimum criterion (the value of λ corresponds to the lowest likelihood deviation) [20]. The riskScore is defined as

$$\text{riskScore} = \sum_{i=1}^{n} Coefficient \times Expression\ .$$

The coefficient is defined as the coefficient derived using LASSO COX regression, and Expression is defined as the expression of important genes.

2.6 Access to Immunotherapy Cohort and Clinical Information

We included in our analysis the IMvigor210 immunotherapy group from prior studies with complete clinical and transcriptome data [21]. The IMvigor210 cohort focuses on the efficacy of an anti-PD-L1 antibody (pembrolizumab) in patients with advanced uroepithelial carcinoma. We downloaded the complete transcriptomic data and detailed clinical information from the relevant URL (http://research-pub.gene.com/ IMvigor210CoreBiologies/). Then, using the R package DEseq2, we normalized the data and transformed the count values to TPM values.

2.7 Chemotherapy drug sensitivity analysis, small molecule drug screening and molecular docking validation

First, we utilized the R package pRRophetic to examine the half-maximal inhibitory concentrations (IC50) of common chemotherapeutic agents and targeted medicines to quantify our riskScore model's prediction power for SKCM treatment. After that, Using the Cmap (Connectivity Map) database, we calculated medications having significantly negative correlations with seven highly elevated genes and then picked the top 10 drugs [22]. Then, we obtained the SDF 2D structure files of the 10 drug candidates from the Pubchem database, transformed the small molecules into 3D structure files using Autodock MGLTools, performed energy optimization, and then exported the files in PDBQT format. We downloaded seven highly up-regulated genes from the PDB database to determine crystal structures; however, CXCL9 and PRF1 were excluded from the subsequent molecular docking investigation because they lacked crystal structure information. The receptor crystal structures were processed in bulk using the prepare_recpetor4.py script in Autodock MGLTools, then docked to small molecules and receptor proteins using Autodock Vina (version 1.1.2). We used Pymol to map the small molecule-protein binding and visualize molecular docking results [23]. The docking scoring heat map was generated using the R package ComplexHeatmap.

2.8 Validation of key molecules in cells and tissues

We utilized the following cell lines to validate key genes in SKCM and normal skin tissues. We employed the A375 human melanoma cell line, SK-MEL-28 human melanoma cell line, human immortalized keratin-forming cell line (Hacat), and human melanocyte cell line (PIG1) in this study. All cells were grown in RPMI-1640 media supplemented with 10% fetal bovine serum in a 37°C, 5% CO_2 atmosphere.

Then, we performed further validation on 10 pairs of SKCM and neighboring normal tissue samples. The Human Research Ethics Committee of the Chinese PLA General Hospital authorized all experimental components, and patients signed informed permission forms. We utilized qRT-PCR to detect the relative expression of seven key genes using conventional techniques [24]. Using Trizol reagent, we extracted total RNA from the four cell lines and tissues listed above. RNA concentration was determined using a NanoDrop spectrophotometer. We synthesized cDNA using PrimerScript 5×RT Master Mix (BioRad), and mRNA expression levels were quantified using a 2×SYBR Green PCR Kit. Utilizing the $2^{-\Delta\Delta Ct}$ approach, we quantified the real-time PCR analysis and determined the relative expression of essential genes individually in cells and human specimen tissues. Beijing Huada Corporation produced all primers. We presented the primer sequences in the ***Supplemental Table***.

2.9 Statistical analysis

We utilized the Wilcoxon test to analyze the differences between the two groups in this study. In comparison, one-way ANOVA and the Kruskal-Wallis test were employed to determine the significance of differences among three or more groups. Spearman's analysis was used for correlation testing. We utilized univariate Cox regression models to construct hazard ratios (HR) and 95 percent confidence

intervals (95%CI), and multivariate Cox model models to investigate the predictive potential of riskScore as an independent prognostic biomarker for assessing patient prognosis. All statistical *P* values in this investigation were two-tailed, and $P<0.05$ was considered statistically significant.

3. Results

3.1 Genomic mapping differences between normal and SKCM

The study's flowchart is depicted in ***Figure 1***. Using cluster analysis and principal component analysis (PCA), we first demonstrated the genetic differences between normal skin tissues and SKCM (***Figure 2A-B***). By comparing 469 SKCM and 556 normal skin tissues, we discovered that the expression of 4555 genes was significantly altered in tumor tissues against normal tissues ($P<0.01$ & $|logFC|\geq2$), with 2296 genes considerably up-regulated and 2259 genes significantly down-regulated (***Figure 2C***). The GO enrichment analysis demonstrates that SKCM genetic variants play a role in TME immune components and matrix-related biological processes, such as cytokine-mediated signaling pathway, cell chemotaxis, and positive regulation of response to external stimulation (***Figure 2D-G***). The KEGG pathway indicates that these genes are also involved in immune-related signaling pathways, such as cytokine-cytokine receptor interaction, viral protein interaction with the cytokine-cytokine receptor, viral protein interaction with cytokine and cytokine receptor, and natural killer cell-mediated cytotoxicity (***Figure 2H***). The heatmap results also imply that immunological and matrix-related pathways play a significant role in the SKCM genome (***Figure 2I***). The PPI network reveals a close interaction between SKCM-related genes at the protein level (***Figure 3A***). We identified a sub-network module with solid predictive value, in which CD86, CXCL9, FCGR3A, GZMB, PRF1, STAT1, and TLR7 were designated as key molecules with high connectedness. We also investigated the protein correlation between these key molecules (***Figure 3B-C***). We found that the expression of critical molecules is significantly elevated in SKCM samples relative to normal samples (***Figure 3D***). We performed dimensionality reduction using PCA to determine if these critical molecules can distinguish SKCM samples from normal samples. We discovered two completely disjoint populations, indicating that the expression patterns of critical molecules in normal and SKCM samples are distinct (***Figure 3E***). In addition, we demonstrated the interaction of numerous immune molecules in the SKCM TME, the signaling cascade and transmission, and the distinct regulation patterns between molecules (***Figure 3F***).

3.2 Multi-omics analysis to identify key molecules and mutation and survival analysis

We obtained immunohistochemistry results for seven critical molecules from the HPA database and qualitatively found protein-level expression variations between normal tissues and SKCM samples (***Figure 4A-B***). In a subsequent confirmation, we evaluated the expression of these important molecules in cell lines and 10 pairs of tumors and surrounding normal tissues to validate the differential and significant expression of essential molecules in SKCM tissues. Spearman correlation analysis identified a significant positive correlation between important molecules and a strong interaction between these molecules (***Figure 4C***). The mutations of SKCM's essential molecules were then studied. 15.42 percent of

patients out of 467 samples had mutations in at least one essential molecule. CD86 had the highest frequency of mutations in SKCM samples, followed by TLR7, and all essential molecules were found with gene mutation (***Figure 4D***). The expression and mutation of these essential molecules may play a crucial role in the growth and metastasis of SKCM, as deduced by our findings. In addition, we probed into the predictive value of key molecules based on an independent SKCM cohort from the TCGA database using survival analysis. The TCGA-SKCM cohort also demonstrated variations in the expression of essential molecules between normal and tumor samples. For survival analysis, 467 SKCM patients with complete clinical annotation were available. Patients with high expression of CD86, CXCL9, FCGR3A, GZMB, PRF1, STAT1, and TLR7 had a significant survival benefit over those with low expression (***Figure 5A-G***). Seven critical molecules displayed significantly greater expression levels in SKCM, and all seven key molecules as protective molecules significantly increased SKCM patient survival.

3.3 Evaluation of immune cell infiltration characteristics of tumor microenvironment

To further investigate the role of identified critical molecules in TME immune cell infiltration in SKCM patients, we analyzed the infiltration of 28 types of TME cells in normal and tumor tissues (***Figure 6A***). T helper cells (type 1 and 2), activated B cells, $CD4^+$ T cells, $CD8^+$ T cells, immature B cells, regulatory T cells, natural killer cell, activated dendritic cell, plasmacytoid dendritic cell, MDSC, monocyte, memory B cell, macrophage, gamma delta T cell, effector memory $CD4^+$ T cells, CD56 dim natural killer cell, immature dendritic cell, eosinophil, $CD8^+$ T cells were highly plentiful in tumor tissue. However, other cell subsets were notably abundant in normal tissue. Then, using the PCA algorithm, we compared the infiltration patterns of TME cells in normal and tumor tissues to determine if there were any differences. After dimensionality reduction, the results demonstrated the existence of two distinct populations of TME cells (***Figure 6B***). Using the ESTIMATE algorithm, we determined the immunological and mesenchymal activity in the SKCM microenvironment. It was discovered that immune and mesenchymal activities were much higher in tumor tissues than normal skin tissues (***Figure 6C-D***). To examine the link between critical molecules and immune cells in the TME, we correlated key molecules with cellular fractions in the TME. Spearman correlation analysis revealed that these molecules were strongly positively linked with most TME cellular fractions, except T helper cells, CD56 bright natural killer cells, and neutrophil cell infiltration (***Figure 6E***). In addition, the expression of seven essential molecules demonstrated a significant positive association with PD-L2 and PD-L1 and a negative correlation with CTLA4 (***Figure 6F***). CTLA4 had the most significant connection with STAT1 and TLR7 (***Figure 6G-H***).

3.4 Correlation model construction for prognosis and immunotherapy based on key molecules

We incorporated patient prognostic information and TME immune cell infiltration status to build the riskScore model, and we integrated the role of these essential molecules using LASSO Cox regression. RiskScore was determined by the expression of the four most representative important molecules, according to the findings (***Figure 7A-B***). Based on the critical value of -7.07 (***Figure 7C***) computed by the MaxStat R package, we classified the patients into high-risk and low-risk groups. We observed that the low-risk group had a considerable survival advantage over the high-risk group (***Figure 7D***). In addition, the

expression of these essential molecules is much higher in low-risk tumors than in high-risk, suggesting that these key molecules have a protective role in the low-risk group, consistent with the findings of our earlier investigation (***Figure 7E-F***). With rising risk, patient mortality might climb significantly (***Figure 7G-H***). Our examination of multivariate COX regression models incorporating basic clinical and pathological information about the patients demonstrated that riskScore could be an independent and robust predictive biomarker to evaluate SKCM patients (***Figure 8A***). In addition, we developed a nomogram that combines the riskScore with independent clinical prognostic indicators to estimate the likelihood of patient mortality (***Figure 8B***). The calibration plots demonstrated that the generated nomogram had a superior prediction ability (***Figure 8C***). We displayed ROC curves based on TCGA data with AUC of 0.757, 0.675, and 0.657 for 1, 2, and 3 years, indicating the riskScore's excellent predictive performance (***Figure 8D***). In addition, our findings demonstrated that riskScore surpassed other clinical factors, such as age and number of nodules, in predicting OS in patients with SKCM (***Figure 8E***).

We utilized gene set enrichment analysis (GSEA) to investigate the activated biological pathways in the low-risk and high-risk groups. Compared to the low-risk group, cancer-related pathways such as P53, PI3K-AKT-mTOR, NOTCH, and WNT were considerably activated in the high-risk group (***Figure 8F-K***). Then we analyzed the difference in TME cell infiltration between the low-risk and high-risk groups, and we discovered that all immune infiltrating cells, except for CD56 dim natural killer cells and CD56 bright natural killer cells, were significantly higher in the low-risk group than in the high-risk group (***Figure 9A***). By correlation analysis, we discovered that riskScore values were strongly and positively linked with the majority of TME cell infiltrating rates (***Figure 9B***). We also discovered a significant and positive correlation between riskScore values and the expression of immune checkpoint molecules, indicating the potential predictive role of riskScore in predicting clinical response to immunotherapy and providing a foundation for developing novel immunotherapies (***Figure 9C***). As immune checkpoint blockade (ICB) has made advances in the treatment of SKCM over the past few years, we verified riskScore's ability to predict the clinical response of patients to ICB therapy. In the IMvigor210 cohort treated with anti-PD-L1 therapy, low-risk patients had a considerable clinical benefit and prolonged survival (***Figure 9D***). The patients with complete remission (CR) or stable disease (SD) had a lower risk (***Figure 9E***). In addition, we noticed that low-risk individuals responded considerably better to PD-L1 blocking therapy than high-risk patients (***Figure 9F***).

3.5 Chemotherapy drug sensitivity analysis, small molecule drug screening and molecular docking validation

We analyzed 20 common chemotherapeutic and targeted medicines and found substantial variations between the high-risk and low-risk categories in IC50 values (***Figure 10 A-T***). The results indicate that our riskScore signature can uncover prospective biomarkers of chemotherapy and targeted medication sensitivity. Then, we calculated the connection between medication-treated expression profiles and highly up-regulated expression profiles of seven key genes using the Cmap database. We then identified the top ten pharmaceuticals with negative correlations as potential treatment candidates (***Table 1***). ***Figure 11A-J*** shows the chemical structures of these ten compounds. AGI-6780 and Zofenopril-calcium bind well to

GZMB, indicating that these two small compounds can be employed as possible target medicines to target GZMB. In addition, we utilized Pymol to generate a heatmap of the binding of CD86, FCGR3A, STAT1, TLR7, and GZMB proteins to the most strongly bound small molecules or the top two most strongly bound small molecules (***Figure 11K***). The results demonstrated that the small molecules of CD86 bound to Baricitinib formed hydrogen bonds with THR-69, SER-67, GLN-16. The binding of FCGR3A to Zofenopril-calcium formed hydrogen bonds with HIS-111 and ARG-109. The binding of GZMB to Zofenopril-calcium formed hydrogen bonds with LYS-113 and ARG-87, and no hydrogen bonds were formed in the binding of AGI-6780. Small molecules in the binding of STAT1 to Calcipotriol formed hydrogen bonds with GLU-353 and GLN-271, and small molecules in the binding of TLR7 to Zofenopril-calcium formed hydrogen bonds mainly with LYS-464. The majority of receptor and ligand binding energies are less than -7 kcal.mol^{-1}, indicating that the target protein and active ingredient can bind spontaneously with high affinity and stable conformation, and thus small molecule medicines are likely to act on these targets. To illustrate the molecular interactions, we chose the small molecule medication with the lowest binding energy to dock the target for docking visualization (***Figure 12A-H***).

Table 1

Results of Cmap analysis

Cmap name	N	Celline	Enrichment	FDR_Q_nlog10
Gabapentin	2	YAPC	-0.94	15.65
Baricitinib	3	HBL1	-0.92	15.65
DPN	3	A549	-0.91	15.65
AGI-6780	2	PC3	-0.9	15.65
Fusaric-acid	3	SKB	-0.9	15.65
Ru-24969	3	MCF7	-0.89	15.65
Calcipotriol	2	HCC515	-0.89	15.65
Fenoterol	2	YAPC	0.89	15.65
Zofenopril-calcium	2	JURKAT	-0.89	15.65
RS-102895	3	A549	-0.89	15.65

3.6 Expression validation of key molecules

We downloaded immunohistochemical staining images of normal and SKCM tissues for the essential genes from the Human Protein Atlas database. We validated the differential expression of these proteins in normal skin tissues and SKCM tissues using semi-quantitative analysis after selecting the appropriate field of view (the first column of ***Figure 13***). qRT-PCR was subsequently utilized to confirm the differential expression of these seven essential genes in four cell lines, Hacat, PIG1, A375, and SK-Mel-14, in 10 pairs

of normal skin and SKCM patients (the second column of ***Figure 13***). The mRNA expression of CD86, CXCL9, FCGR3A, GZMB, PRF1, STAT1, and TLR7 was considerably higher in the A375 and SK-Mel-14 cell lines than in the Hacat and PIG1 cell lines. We discovered that the patients' mRNA expression of CD86, CXCL9, FCGR3A, GZMB, PRF1, STAT1, and TLR7 was much higher in SKCM than in normal skin tissue (the third column of ***Figure 13***). Using experimental validation at the mRNA and protein levels, we determined that CD86, CXCL9, FCGR3A, GZMB, PRF1, STAT1, and TLR7 were differentially expressed in normal skin tissues and SKCM and inferred that these key molecules could be potentially critical targets for the treatment of SKCM.

4. Discussion

In recent years, the incidence of SKCM, a highly aggressive skin tumor, has increased globally at an alarming rate. Melanoma cells tend to migrate to distant places and evade immune system control. In recent years, chemotherapy, immunotherapy, and targeted therapies have been utilized to increase the survival rate of patients with advanced melanoma; nonetheless, there are still issues such as high drug resistance, low drug sensitivity, and poor prognosis [25]. In recent years, substantial advancements in sequencing technologies have created new options for methodically deciphering key genes and epigenetic alterations in various kinds of SKCM. We combined immune-related gene sets and multiple datasets to explore the complex integrative roles of multiple key molecules on TME infiltration and heterogeneity. This study revealed the potential mechanisms of TME anti-tumor immune response, screened potential biological therapeutic targets and therapeutic agents, and thus accurately predicted or identified patient response to immunotherapy.

We investigated the key molecules affecting patient prognosis in the present study using 469 SKCM samples and 556 normal skin samples with multiple database gene sets. By studying the genetic changes between normal skin tissues and SKCM tissues, we discovered that immune-related pathways, such as cytokine-mediated signaling and cell chemotaxis systems, exhibited significant differences. We chose the most predictive sub-network modules from the PPI network and employed seven key molecules with high interaction as the foundation of the prediction model. Analysis of mutations revealed that at least 15.42% of patients had mutations in at least one gene and that all essential molecules were mutated in SKCM, with CD86 mutations occurring most frequently. The expression of these seven essential genes was dramatically elevated in tumor tissue as protective genes and was highly correlated with a significantly more extended survival period. Through immune-related analysis, we determined that SKCM had much higher immune cell infiltration levels than normal skin and significantly higher total immunological and mesenchymal activity, which significantly altered the microenvironment's infiltration pattern. The expression of seven essential molecules was significantly and positively connected with the infiltration of 28 TME cells, as determined by a subsequent investigation into the association between key molecules and TME cell infiltration levels. In addition, we discovered that important molecules were positively connected with PD-L1/L2 expression and negatively correlated with CTLA4 and PD-1 expression. We used the LASSO COX regression model to develop the riskScore model. We discovered that low-risk patients had more significant TME immune cell infiltration and a longer survival time. We

also discovered that riskScore could be utilized as an independent biomarker to assess patient prognosis by multivariate COX regression. We integrated riskScore and independent clinical prognostic markers to generate nomogram plots that displayed excellent predictive performance. In addition, the vital link between riskScore and immunological checkpoints shows that it can predict a patient's immunotherapy response. In the IMvigor210 group receiving anti-PD-L1 therapy, we observed a significant therapeutic benefit with increased survival time and enhanced clinical response in low-risk patients compared to those at high risk. In addition, using small molecule drug screening and molecular docking, Gabapentin and Baricitinib were discovered as prospective small-molecule medicines to treat SKCM. Finally, we utilized IHC and qRT-PCR to confirm the expression of important molecules.

The prognostic model developed in this study consists of seven key molecules, CD86, CXCL9, FCGR3A, GZMB, PRF1, STAT1, and TLR7, all of which are expressed up-regulated in SKCM as protective molecules. CD86 (cluster of differentiation 86), a member of the immunoglobulin superfamily, interacts with the inducer CD28 and the inhibitor CTLA4 and functions as a crucial cofactor in the stimulation of T-lymphocyte proliferation and IL-2 production [26]. CTLA4, an immunological checkpoint molecule, can influence the TME of SKCM by binding to B7 (CD80/CD86) molecules on melanoma antigen-presenting cells to down-regulate T cell activation [27]. The chemokine CXCL9 (C-X-C motif chemokine ligand 9) correlates positively with CD8+ T cell infiltration in solid malignancies [28] [29]. CXCL9 is abundantly expressed in several solid tumors, including SKCM, and it stimulates the infiltration of $CD4^{+}$T and $CD8^{+}$T lymphocytes into tumor cell regions, so boosting the response of cytotoxic T lymphocytes and thereby killing tumor cells [30] [31]. In addition, CXCL9 can assist in identifying individuals whose tumors are invaded by activated T cells, hence enhancing the efficacy of immunotherapies such as anti-PD1 [32] [33]. FCGR3A (Fc fragment of IgG receptor IIIa) encodes the receptor for the Fc region of immunoglobulin G. It is implicated in eliminating antigen-antibody complexes and other antibody-dependent responses [34] [35]. FCGR3A interacts with FCGR1A in numerous pathophysiological processes and is substantially related with overall survival (OS) in SKCM, renal clear cell carcinoma, and other malignancies [36]. Granzyme B (GZMB) is an exogenous serine protease generated from granules released by cytotoxic lymphocytes (CTLs) and natural killer cells (NK) [37]. GZMB has been discovered to be related with NK cell treatment in individuals with SKCM. By evaluating NK cells in the blood of SKCM patients, it was discovered that NK cells entering metastatic melanoma tissue have a diminished cytotoxic capacity due to decreased expression of GZMB and perforin [38]. PRF1 (perforin 1) encodes a protein structurally similar to complement C9, which plays a crucial function in immunity. This protein facilitates the release of granzyme and the subsequent lysis of target cells by creating membrane holes [39] [40]. Tumors of SKCM patients treated with the anti-PD1 medication nivolumab demonstrated dramatically higher levels of PRF1, CD8, and GZMA, as well as an enhanced TBX21/GATA3 ratio, according to research. This suggests that PRF1 mediates tumor-infiltrating T lymphocytes (TIL) oligoclonal amplification-enhanced Th1 (helper T cell type I)-skewed cellular immunity during nivolumab treatment [41]. STAT1 (signal transducers and activators of transcription 1) is a family of cytosolic proteins that, upon activation, can translocate to the nucleus and bind DNA, which has dual signal transduction and transcriptional control functions [42] [43]. Hypermethylation in the promoter region of the SOCS3 gene was discovered to reduce

SOCS3 protein expression in some SKCM patients. The greater the sensitivity of melanoma cells to IFN-γ, the lower the expression of SOCS3, and the lowering of SOCS3 expression in melanoma cells by IFN-γ may significantly stimulate the production of STAT1 [44], Overexpression of a dominant-negative STAT1 plasmid completely derepressed the growth inhibition induced by IFN-γ in melanoma cells [45]. TLR7 (toll-like receptors 7) is an endosomal pattern recognition receptor, when activated, causes type I interferons and inflammatory reactions [46]. TLR7 plays a crucial role in activating both natural and acquired immune responses and has an activating effect on virtually all cells engaged in the tumor immune response [47]. It was discovered that chemically coupling ibrutinib with TLR7 receptor agonists to produce novel immune-targeting complexes called GY161 increased the levels of $CD8^+$ T cells in spleen and tumor in vivo. GY161 inhibited the growth of B16 melanoma cell-derived tumors and prolonged the survival time of mice [48].

The significance of the TME in tumor development is critical. Numerous studies have demonstrated that different immune cells can operate as tumor promoters or tumor antagonists in various tumors [49] [50]. Therefore, it is necessary to do additional research on immune infiltration in TME better to comprehend the relationship between immune components and tumor progression. After constructing a riskScore model to divide the high- and low-risk groups, we discovered that the expression of seven protective key molecules was significantly lower in the high-risk group. In contrast, immune cell infiltration was significantly lower in the high-risk group compared to the low-risk group. We discovered that the group at low risk had more extensive levels of $CD4^+$ and $CD8^+$ T cells. $CD8^+$ T cells eliminate tumor cells based on cell differentiation and invasion. They can differentiate into effector and cytotoxic T cells to perform anti-tumor actions in the tumor-infiltrating microenvironment [51]. In secondary lymphoid organs, $CD4^+$ T cells can inhibit or stimulate the activity of anti-tumor cytotoxic T cells, hence modulating tumor cells. Tumor infiltration lymphocytes (TILs) in SKCM are a potential immunotherapy target in the future. [52]

The innovative use of traditional drugs has now become an important strategy for antineoplastic drug development. The discovery of potential mechanisms of conventional medications can save time and money while also enhancing the security of drug administration. Gabapentin and Baricitinib promise medications for the treatment of SKCM, per the CMAP database. Gabapentin, whose mechanism of action is currently unknown, is commonly believed to modify the GABA metabolic pathway in patients with circumscribed seizures that are not adequately controlled or tolerated by traditional antiepileptic medicines. Several investigations have verified the anticancer effects of Gabapentin in recent years. Gabapentin may achieve anti-melanoma effects in mice by reducing cell proliferation, CCL2 production, and calcium influx [53]. In recent years, it has been demonstrated that thiamine-dependent enzymes (TDEs) are frequently tumor-related targets due to their control of metabolic pathways that are frequently altered in cancer. Gabapentin can impede the growth of TDEs, resulting in a tumor-killing mechanism of toxicity [54]. Through molecular docking analysis and the summary of key molecules mentioned above, we found that Gabapentin most likely acts through STAT1 and TLR7 to achieve anti-tumor effects by altering the immune infiltration content of TILs such as $CD8^+$ T cells in TME to inhibit the proliferation and invasion of SKCM cells.

In conclusion, the riskScore model developed in this study can be utilized as an independent and reliable biomarker to predict the prognosis of individuals with SKCM. In addition, we screened and predicted small-molecule pharmaceuticals. This study not only provides riskScore models that can predict patient prognosis and assess the heterogeneity and complexity of TME cell infiltration, but it also contributes to the development and guidance of novel immune combination therapy strategies and the promotion of the development of personalized tumor immunotherapy and precision medicine.

Declarations

Ethics approval and consent to participate:

Following permission from the Chinese PLA General Hospital's Human Research Ethics Committee, we collected ten pairs of SKCM and para-cancerous normal tissue specimens. Written informed consent was obtained from individual or guardian participants.

Consent for publication

Not applicable.

Availability of data and material

All data generated or analyzed during this study are included in this published article and its supplementary files.

Competing interests

The authors declare that they have no competing interests.

Funding

Not applicable.

Authors' contributions

Jiahua Xing and *Ziqi Jia* wrote the main manuscript text and all the figures, *Yan Li* and *Yan Han* suggested ideas and steps for the article, and participated in the revision of part of the article. All authors read and approved the final manuscript.

Acknowledgements

Not applicable.

References

1. R.L. Siegel, K.D. Miller, H.E. Fuchs, A. Jemal, Cancer Statistics, 2021, CA: a cancer journal for clinicians, 71 (2021) 7-33.
2. R.E. Hunger, S.M. Seyed Jafari, S. Angermeier, M. Shafighi, Excision of fascia in melanoma thicker than 2 mm: no evidence for improved clinical outcome, The British journal of dermatology, 171 (2014) 1391-1396.
3. S. Felton, R.S. Taylor, D. Srivastava, Excision Margins for Melanoma In Situ on the Head and Neck, Dermatologic surgery : official publication for American Society for Dermatologic Surgery [et al.], 42 (2016) 327-334.
4. R.A. Scolyer, R.V. Rawson, J.E. Gershenwald, P.M. Ferguson, V.G. Prieto, Melanoma pathology reporting and staging, Modern pathology : an official journal of the United States and Canadian Academy of Pathology, Inc, 33 (2020) 15-24.
5. L.E. Haydu, S.N. Lo, J.L. McQuade, R.N. Amaria, J. Wargo, M.I. Ross, J.N. Cormier, A. Lucci, J.E. Lee, S.D. Ferguson, R.P.M. Saw, A.J. Spillane, K.F. Shannon, J.R. Stretch, P. Hwu, S.P. Patel, A. Diab, M.K.K. Wong, I.C. Glitza Oliva, H. Tawbi, M.S. Carlino, A.M. Menzies, G.V. Long, A.J. Lazar, M.T. Tetzlaff, R.A. Scolyer, J.E. Gershenwald, J.F. Thompson, M.A. Davies, Cumulative Incidence and Predictors of CNS Metastasis for Patients With American Joint Committee on Cancer 8th Edition Stage III Melanoma, Journal of clinical oncology : official journal of the American Society of Clinical Oncology, 38 (2020) 1429-1441.
6. M. Matias, J.O. Pinho, M.J. Penetra, G. Campos, C.P. Reis, M.M. Gaspar, The Challenging Melanoma Landscape: From Early Drug Discovery to Clinical Approval, Cells, 10 (2021).
7. L. Yang, Y. Xu, Y. Yan, P. Luo, S. Chen, B. Zheng, W. Yan, Y. Chen, C. Wang, Common Nevus and Skin Cutaneous Melanoma: Prognostic Genes Identified by Gene Co-Expression Network Analysis, Genes, 10 (2019).
8. C. Karimkhani, A.C. Green, T. Nijsten, M.A. Weinstock, R.P. Dellavalle, M. Naghavi, C. Fitzmaurice, The global burden of melanoma: results from the Global Burden of Disease Study 2015, The British journal of dermatology, 177 (2017) 134-140.
9. R.G. Witt, D.J. Erstad, J.A. Wargo, Neoadjuvant therapy for melanoma: rationale for neoadjuvant therapy and pivotal clinical trials, Therapeutic advances in medical oncology, 14 (2022) 17588359221083052.
10. J.R. Dixon-Douglas, R.P. Patel, P.M. Somasundram, G.A. McArthur, Triplet Therapy in Melanoma - Combined BRAF/MEK Inhibitors and Anti-PD-(L)1 Antibodies, Current oncology reports, (2022).
11. P.F. Ferrucci, M. Lens, E. Cocorocchio, Combined BRAF-Targeted Therapy with Immunotherapy in BRAF-Mutated Advanced Melanoma Patients, Current oncology reports, 23 (2021) 138.
12. H.R. Ali, L. Chlon, P.D. Pharoah, F. Markowetz, C. Caldas, Patterns of Immune Infiltration in Breast Cancer and Their Clinical Implications: A Gene-Expression-Based Retrospective Study, PLoS medicine, 13 (2016) e1002194.
13. A.M. Newman, C.L. Liu, M.R. Green, A.J. Gentles, W. Feng, Y. Xu, C.D. Hoang, M. Diehn, A.A. Alizadeh, Robust enumeration of cell subsets from tissue expression profiles, Nature methods, 12 (2015) 453-

457.

14. M. Angelova, P. Charoentong, H. Hackl, M.L. Fischer, R. Snajder, A.M. Krogsdam, M.J. Waldner, G. Bindea, B. Mlecnik, J. Galon, Z. Trajanoski, Characterization of the immunophenotypes and antigenomes of colorectal cancers reveals distinct tumor escape mechanisms and novel targets for immunotherapy, Genome biology, 16 (2015) 64.
15. F.R. Greten, S.I. Grivennikov, Inflammation and Cancer: Triggers, Mechanisms, and Consequences, Immunity, 51 (2019) 27-41.
16. M.E. Ritchie, B. Phipson, D. Wu, Y. Hu, C.W. Law, W. Shi, G.K. Smyth, limma powers differential expression analyses for RNA-sequencing and microarray studies, Nucleic acids research, 43 (2015) e47.
17. W.P. Bandettini, P. Kellman, C. Mancini, O.J. Booker, S. Vasu, S.W. Leung, J.R. Wilson, S.M. Shanbhag, M.Y. Chen, A.E. Arai, MultiContrast Delayed Enhancement (MCODE) improves detection of subendocardial myocardial infarction by late gadolinium enhancement cardiovascular magnetic resonance: a clinical validation study, Journal of cardiovascular magnetic resonance : official journal of the Society for Cardiovascular Magnetic Resonance, 14 (2012) 83.
18. D.A. Barbie, P. Tamayo, J.S. Boehm, S.Y. Kim, S.E. Moody, I.F. Dunn, A.C. Schinzel, P. Sandy, E. Meylan, C. Scholl, S. Fröhling, E.M. Chan, M.L. Sos, K. Michel, C. Mermel, S.J. Silver, B.A. Weir, J.H. Reiling, Q. Sheng, P.B. Gupta, R.C. Wadlow, H. Le, S. Hoersch, B.S. Wittner, S. Ramaswamy, D.M. Livingston, D.M. Sabatini, M. Meyerson, R.K. Thomas, E.S. Lander, J.P. Mesirov, D.E. Root, D.G. Gilliland, T. Jacks, W.C. Hahn, Systematic RNA interference reveals that oncogenic KRAS-driven cancers require TBK1, Nature, 462 (2009) 108-112.
19. K. Yoshihara, M. Shahmoradgoli, E. Martínez, R. Vegesna, H. Kim, W. Torres-Garcia, V. Treviño, H. Shen, P.W. Laird, D.A. Levine, S.L. Carter, G. Getz, K. Stemke-Hale, G.B. Mills, R.G. Verhaak, Inferring tumour purity and stromal and immune cell admixture from expression data, Nature communications, 4 (2013) 2612.
20. J. Gao, P.W. Kwan, D. Shi, Sparse kernel learning with LASSO and Bayesian inference algorithm, Neural networks : the official journal of the International Neural Network Society, 23 (2010) 257-264.
21. S. Mariathasan, S.J. Turley, D. Nickles, A. Castiglioni, K. Yuen, Y. Wang, E.E. Kadel, III, H. Koeppen, J.L. Astarita, R. Cubas, S. Jhunjhunwala, R. Banchereau, Y. Yang, Y. Guan, C. Chalouni, J. Ziai, Y. Şenbabaoğlu, S. Santoro, D. Sheinson, J. Hung, J.M. Giltnane, A.A. Pierce, K. Mesh, S. Lianoglou, J. Riegler, R.A.D. Carano, P. Eriksson, M. Höglund, L. Somarriba, D.L. Halligan, M.S. van der Heijden, Y. Loriot, J.E. Rosenberg, L. Fong, I. Mellman, D.S. Chen, M. Green, C. Derleth, G.D. Fine, P.S. Hegde, R. Bourgon, T. Powles, TGFβ attenuates tumour response to PD-L1 blockade by contributing to exclusion of T cells, Nature, 554 (2018) 544-548.
22. J. Lamb, The Connectivity Map: a new tool for biomedical research, Nature reviews. Cancer, 7 (2007) 54-60.
23. F. Gaudreault, L.P. Morency, R.J. Najmanovich, NRGsuite: a PyMOL plugin to perform docking simulations in real time using FlexAID, Bioinformatics (Oxford, England), 31 (2015) 3856-3858.

24. J. Jozefczuk, J. Adjaye, Quantitative real-time PCR-based analysis of gene expression, Methods in enzymology, 500 (2011) 99-109.
25. B. Domingues, J.M. Lopes, P. Soares, H. Pópulo, Melanoma treatment in review, ImmunoTargets and therapy, 7 (2018) 35-49.
26. A. Naimi, R.N. Mohammed, A. Raji, S. Chupradit, A.V. Yumashev, W. Suksatan, M.N. Shalaby, L. Thangavelu, S. Kamrava, N. Shomali, A.D. Sohrabi, A. Adili, A. Noroozi-Aghideh, E. Razeghian, Tumor immunotherapies by immune checkpoint inhibitors (ICIs); the pros and cons, Cell communication and signaling : CCS, 20 (2022) 44.
27. M.C. Kirchberger, S. Ugurel, J. Mangana, M.V. Heppt, T.K. Eigentler, C. Berking, D. Schadendorf, G. Schuler, R. Dummer, L. Heinzerling, MEK inhibition may increase survival of NRAS-mutated melanoma patients treated with checkpoint blockade: Results of a retrospective multicentre analysis of 364 patients, European journal of cancer (Oxford, England : 1990), 98 (2018) 10-16.
28. H. Liu, Z. Hu, H. Chen, Y. Yan, Z. Le, C. Wei, W. Cao, T. Chen, Y. Chen, L. Liu, Self-degradable poly(β-amino ester)s promote endosomal escape of antigen and agonist, Journal of controlled release : official journal of the Controlled Release Society, 345 (2022) 91-100.
29. C. Wang, J. Shi, J. Xu, Q. Fu, Y. Ding, J. Yang, B. Liu, Q. Gao, J. Qin, C. Liang, NLRC3 High Expression Represents a Novel Predictor for Positive Overall Survival Correlated With CCL5 and CXCL9 in HCC Patients, Frontiers in oncology, 12 (2022) 815326.
30. M.L. Carbone, G. Madonna, A. Capone, M. Bove, S. Mastroeni, L. Levati, M. Capone, P.A. Ascierto, F. De Galitiis, S. D'Atri, C. Fortes, E. Volpe, C.M. Failla, Vitiligo-specific soluble biomarkers as early indicators of response to immune checkpoint inhibitors in metastatic melanoma patients, Scientific reports, 12 (2022) 5448.
31. E.S. Borden, A.C. Adams, K.H. Buetow, M.A. Wilson, J.E. Bauman, C. Curiel-Lewandrowski, H.S. Chow, B.J. LaFleur, K.T. Hastings, Shared Gene Expression and Immune Pathway Changes Associated with Progression from Nevi to Melanoma, Cancers, 14 (2021).
32. K. Masuhiro, M. Tamiya, K. Fujimoto, S. Koyama, Y. Naito, A. Osa, T. Hirai, H. Suzuki, N. Okamoto, T. Shiroyama, K. Nishino, Y. Adachi, T. Nii, Y. Kinugasa-Katayama, A. Kajihara, T. Morita, S. Imoto, S. Uematsu, T. Irie, D. Okuzaki, T. Aoshi, Y. Takeda, T. Kumagai, T. Hirashima, A. Kumanogoh, Bronchoalveolar lavage fluid reveals factors contributing to the efficacy of PD-1 blockade in lung cancer, JCI insight, (2022).
33. R. Cao, L. Cui, J. Zhang, X. Ren, B. Cheng, J. Xia, Immune-related lncRNA classification of head and neck squamous cell carcinoma, Cancer cell international, 22 (2022) 25.
34. M. Moraru, A. Perez-Portilla, K. Al-Akioui Sanz, A. Blazquez-Moreno, A. Arnaiz-Villena, H.T. Reyburn, C. Vilches, FCGR Genetic Variation in Two Populations From Ecuador Highlands-Extensive Copy-Number Variation, Distinctive Distribution of Functional Polymorphisms, and a Novel, Locally Common, Chimeric FCGR3B/A (CD16B/A) Gene, Frontiers in immunology, 12 (2021) 615645.
35. M. Freitas Monteiro, M. Papaserafeim, A. Réal, G.L. Puga Yung, J.D. Seebach, Anti-CD20 rituximab IgG1, IgG3, and IgG4 but not IgG2 subclass trigger Ca(2+) mobilization and cytotoxicity in human NK

cells, Journal of leukocyte biology, 108 (2020) 1409-1423.

36. J.L. Xu, Y. Guo, FCGR1A Serves as a Novel Biomarker and Correlates With Immune Infiltration in Four Cancer Types, Frontiers in molecular biosciences, 7 (2020) 581615.
37. C. Lu, J.D. Klement, A.D. Smith, D. Yang, J.L. Waller, D.D. Browning, D.H. Munn, K. Liu, p50 suppresses cytotoxic T lymphocyte effector function to regulate tumor immune escape and response to immunotherapy, Journal for immunotherapy of cancer, 8 (2020).
38. N.D. Marin, B.A. Krasnick, M. Becker-Hapak, L. Conant, S.P. Goedegebuure, M.M. Berrien-Elliott, K.J. Robbins, J.A. Foltz, M. Foster, P. Wong, C.C. Cubitt, J. Tran, C.B. Wetzel, M. Jacobs, A.Y. Zhou, D. Russler-Germain, L. Marsala, T. Schappe, R.C. Fields, T.A. Fehniger, Memory-like Differentiation Enhances NK Cell Responses to Melanoma, Clinical cancer research : an official journal of the American Association for Cancer Research, 27 (2021) 4859-4869.
39. G.H. Zhu, L.P. Zhang, Z.G. Li, A. Wei, Y. Yang, Y. Tian, H.H. Ma, D. Wang, X.X. Zhao, Y.Z. Zhao, N. Li, W. Liu, T.Y. Wang, R. Zhang, Associations between PRF1 Ala91Val polymorphism and risk of hemophagocytic lymphohistiocytosis: a meta-analysis based on 1366 subjects, World journal of pediatrics : WJP, 16 (2020) 598-606.
40. C.B. Crayne, S. Albeituni, K.E. Nichols, R.Q. Cron, The Immunology of Macrophage Activation Syndrome, Frontiers in immunology, 10 (2019) 119.
41. H. Inoue, J.H. Park, K. Kiyotani, M. Zewde, A. Miyashita, M. Jinnin, Y. Kiniwa, R. Okuyama, R. Tanaka, Y. Fujisawa, H. Kato, A. Morita, J. Asai, N. Katoh, K. Yokota, M. Akiyama, H. Ihn, S. Fukushima, Y. Nakamura, Intratumoral expression levels of PD-L1, GZMA, and HLA-A along with oligoclonal T cell expansion associate with response to nivolumab in metastatic melanoma, Oncoimmunology, 5 (2016) e1204507.
42. B. Rah, R.A. Rather, G.R. Bhat, A.B. Baba, I. Mushtaq, M. Farooq, T. Yousuf, S.B. Dar, S. Parveen, R. Hassan, F. Mohammad, I. Qassim, A. Bhat, S. Ali, M.H. Zargar, D. Afroze, JAK/STAT Signaling: Molecular Targets, Therapeutic Opportunities, and Limitations of Targeted Inhibitions in Solid Malignancies, Frontiers in pharmacology, 13 (2022) 821344.
43. F. Erdogan, T.B. Radu, A. Orlova, A.K. Qadree, E.D. de Araujo, J. Israelian, P. Valent, S.M. Mustjoki, M. Herling, R. Moriggl, P.T. Gunning, JAK-STAT core cancer pathway: An integrative cancer interactome analysis, Journal of cellular and molecular medicine, 26 (2022) 2049-2062.
44. M. Fojtova, V. Boudny, A. Kovarik, L. Lauerova, L. Adamkova, K. Souckova, J. Jarkovsky, J. Kovarik, Development of IFN-gamma resistance is associated with attenuation of SOCS genes induction and constitutive expression of SOCS 3 in melanoma cells, British journal of cancer, 97 (2007) 231-237.
45. M. Kortylewski, W. Komyod, M.E. Kauffmann, A. Bosserhoff, P.C. Heinrich, I. Behrmann, Interferon-gamma-mediated growth regulation of melanoma cells: involvement of STAT1-dependent and STAT1-independent signals, The Journal of investigative dermatology, 122 (2004) 414-422.
46. X. Li, X. Sun, X. Guo, X. Li, S. Peng, X. Mu, Chemical reagents modulate nucleic acid-activated toll-like receptors, Biomedicine & pharmacotherapy = Biomedecine & pharmacotherapie, 147 (2022) 112622.

47. T. Tsubata, Role of inhibitory B cell co-receptors in B cell self-tolerance to non-protein antigens, Immunological reviews, 307 (2022) 53-65.
48. S. Ren, X. Wang, G. Jin, Conjugate of ibrutinib with a TLR7 agonist suppresses melanoma progression and enhances antitumor immunity, International journal of biological sciences, 18 (2022) 166-179.
49. X. Lei, Y. Lei, J.K. Li, W.X. Du, R.G. Li, J. Yang, J. Li, F. Li, H.B. Tan, Immune cells within the tumor microenvironment: Biological functions and roles in cancer immunotherapy, Cancer letters, 470 (2020) 126-133.
50. K.E. Pauken, E.J. Wherry, SnapShot: T Cell Exhaustion, Cell, 163 (2015) 1038-1038.e1031.
51. N.S. Butler, J.C. Nolz, J.T. Harty, Immunologic considerations for generating memory CD8 T cells through vaccination, Cellular microbiology, 13 (2011) 925-933.
52. D.M. Pardoll, S.L. Topalian, The role of CD4+ T cell responses in antitumor immunity, Current opinion in immunology, 10 (1998) 588-594.
53. B.E. Brito, M.A. García, Y.M. De Gouveia, P. Bolaños, S. Devis, G. Bernal, V.A. Tortorici-Brito, L. Baute, G. Díaz-Serrano, V. Tortorici, Concomitant Antihyperalgesic and Antitumor Effects of Gabapentin in a Murine Cancer Pain Model, International journal of molecular sciences, 22 (2021).
54. S. Liu, S. Miriyala, M.A. Keaton, C.T. Jordan, C. Wiedl, D.K. Clair, J.A. Moscow, Metabolic effects of acute thiamine depletion are reversed by rapamycin in breast and leukemia cells, PloS one, 9 (2014) e85702.

Figures

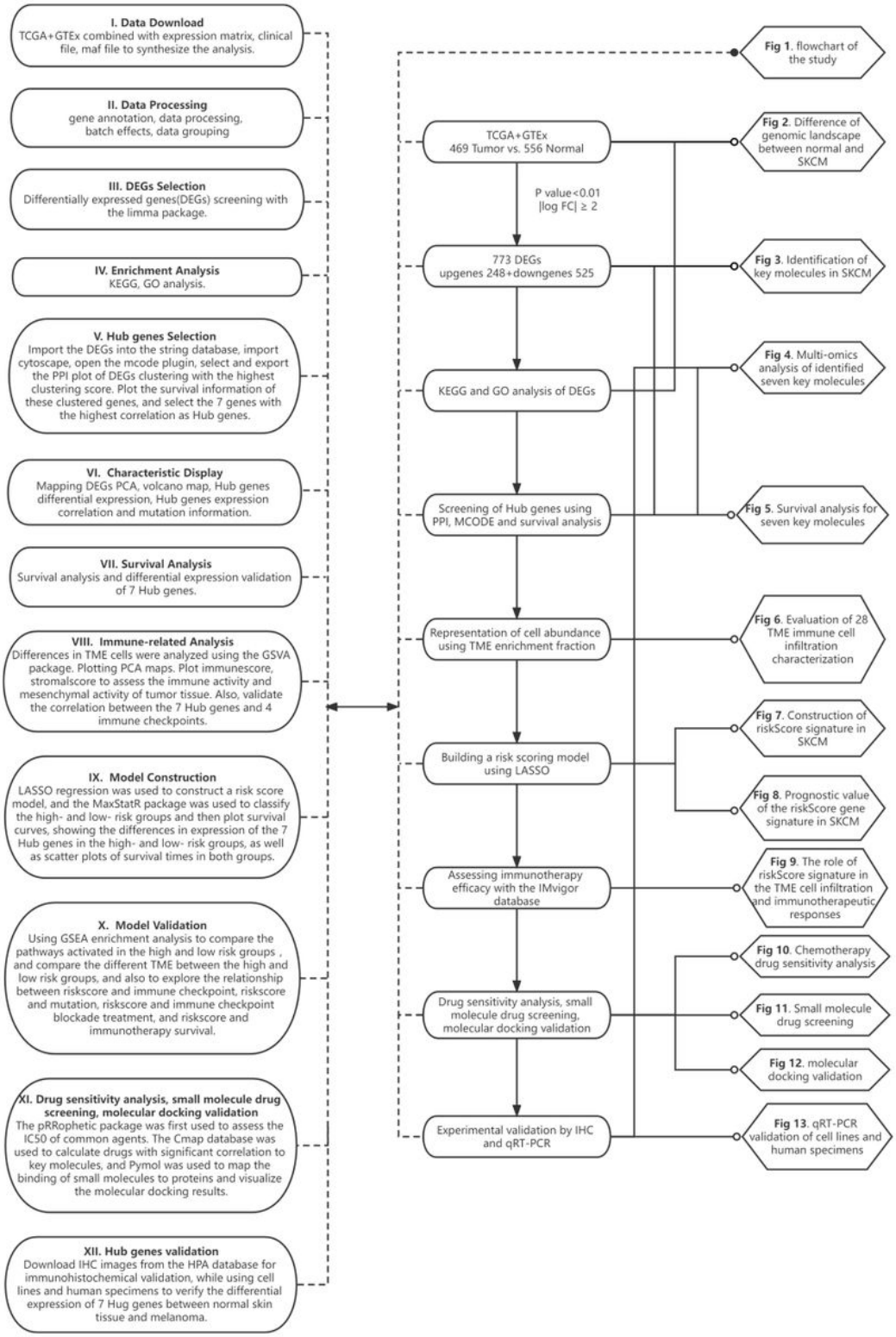

Figure 1

the flowchart of this study.

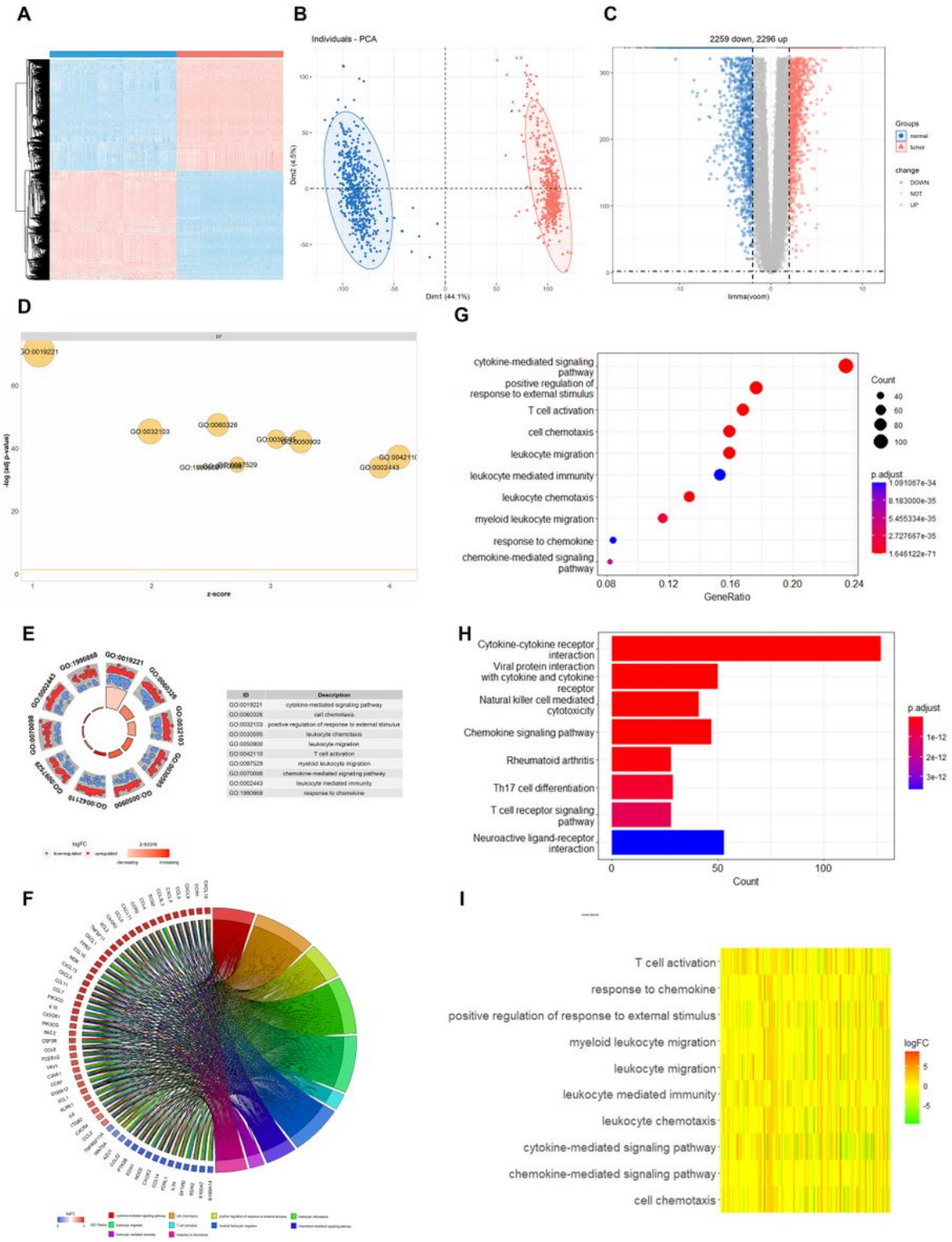

Figure 2

Difference of genomic landscape between normal and skin cutaneous melanoma. (A) Hierarchical clustering of differentially expressed genes between normal and skin cutaneous melanoma samples. Red represents up-regulated and blue represents down-regulated. (B) PCA visualization of differentially expressed genes. (C)Volcano plot of differentially expressed genes. (D) Biological processes enrichment of gene ontology functional enrichment. (E) Molecular function enrichment of gene ontology functional

enrichment. (F) Chord plot of gene ontology functional enrichment. The left half-circle indicates that the genes are sorted by |logFC| and the right half-circle indicates that the gene ontology enrichment analysis term is sorted by strong and weak variation. Red represents up-regulation and blue represents down-regulation, and color shades represent fold change. (G) Cellular component enrichment of gene ontology functional enrichment. (H) KEGG pathway enrichment analyses for differentially expressed genes. All enriched pathways were significant and the color depth represented enriched adjusted *P* value. (I) Heatmap of differentially expressed genes between normal and skin cutaneous melanoma samples. Different colors represent different interaction strength relationships.

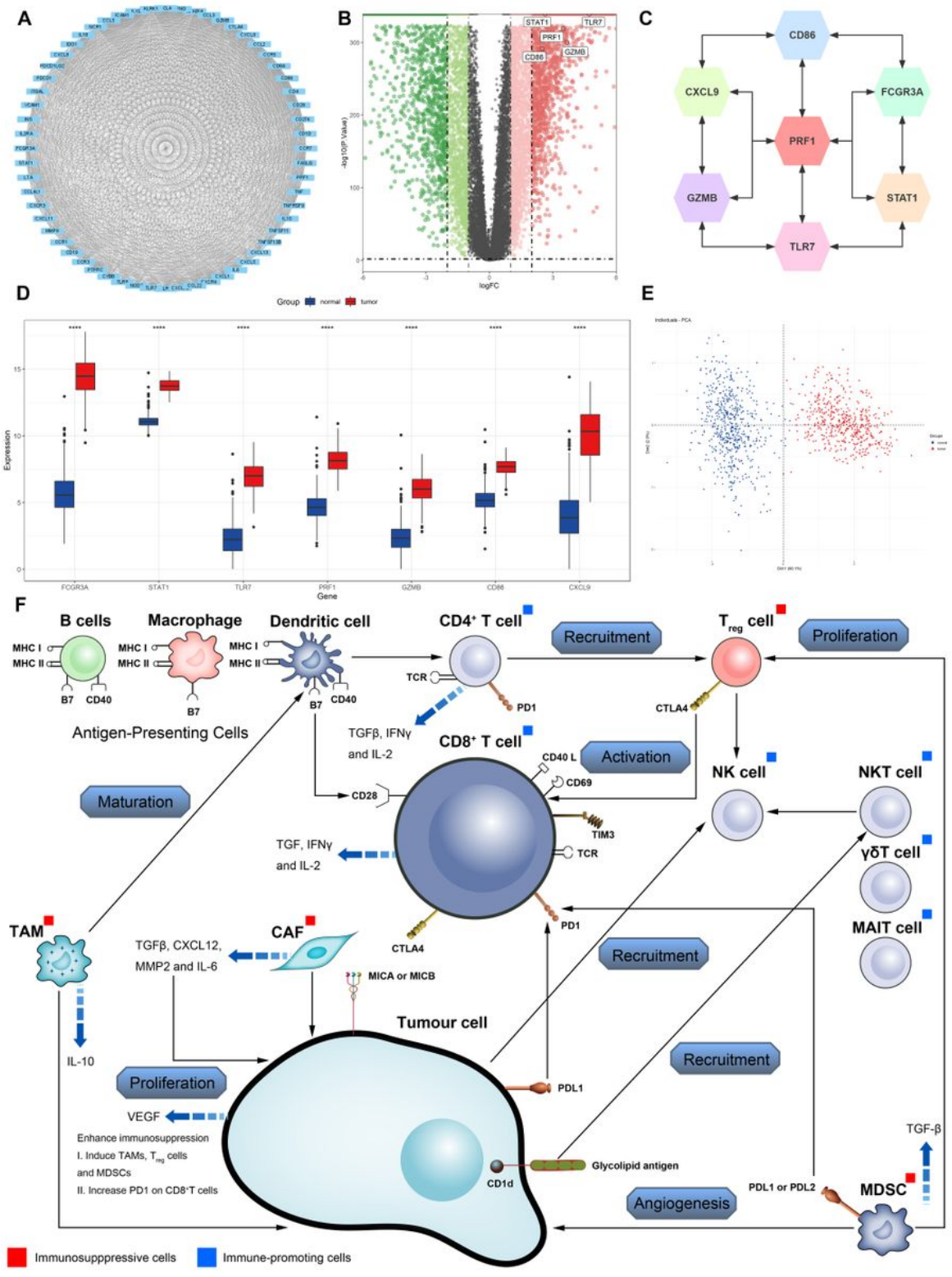

Figure 3

Identification of key molecules in skin cutaneous melanoma. (A) Construction of protein-protein interaction (PPI) network among differentially expressed genes. (B) Volcano plot constructed with the cut-off criterion $P<0.05$ and $|logFC|\geq 1$. (C) The relationship among the seven key molecules at the protein level, each gene is closely linked to each other at the protein level. (D) The seven key molecules expressed in the normal skin and skin cutaneous melanoma (*$P<0.05$, **$P<0.01$, ***$P<0.001$, ****$P<0.0001$). (E)

Principal component analysis for the key molecules revealed. This result shows that seven key molecules can distinguish very well between normal skin and skin cutaneous melanoma. (F) Effect of immune and stromal cells on melanoma tumours.

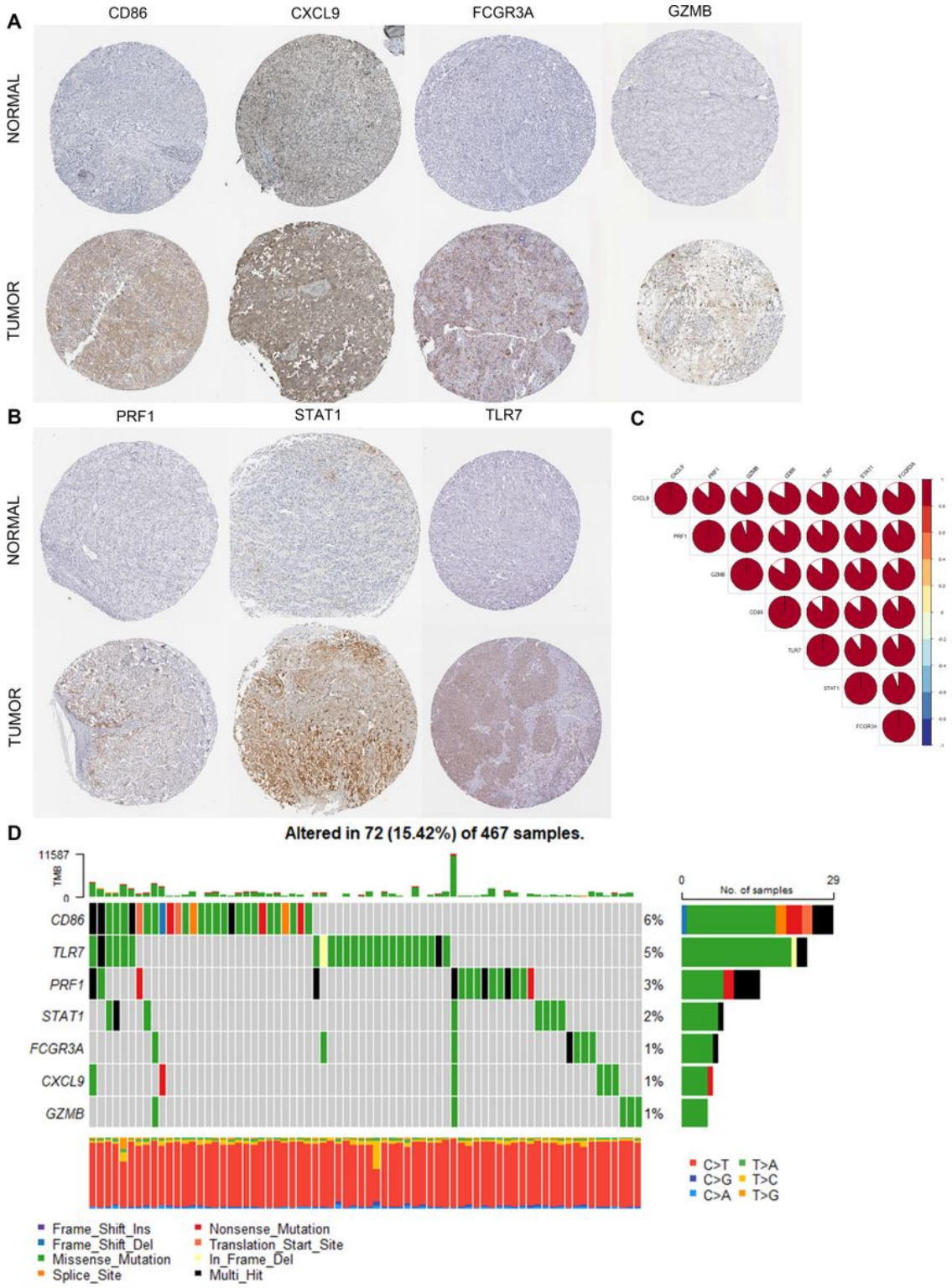

Figure 4

Multi-omics analysis of identified seven key molecules. (A-B) The immunohistochemical staining results revealed significant differences of key molecules (CD86, CXCL9, FCRG3A, GZMB, PRF1, STAT1, TLR7) at the protein expression between normal skin and skin cutaneous melanoma obtained at the Human Proteins Atlas. (C) The correlation between the seven key molecules using spearman analysis. The color area represents the magnitude of correlation intensity, red represents positive correlation and blue represents negative correlation. The key molecules in the figure show very good correlation with each other. (D) Mutation landscape of seven key molecules in 467 samples of TCGA-SKCM cohort. Different color modules represent different molecular mutation frequencies.

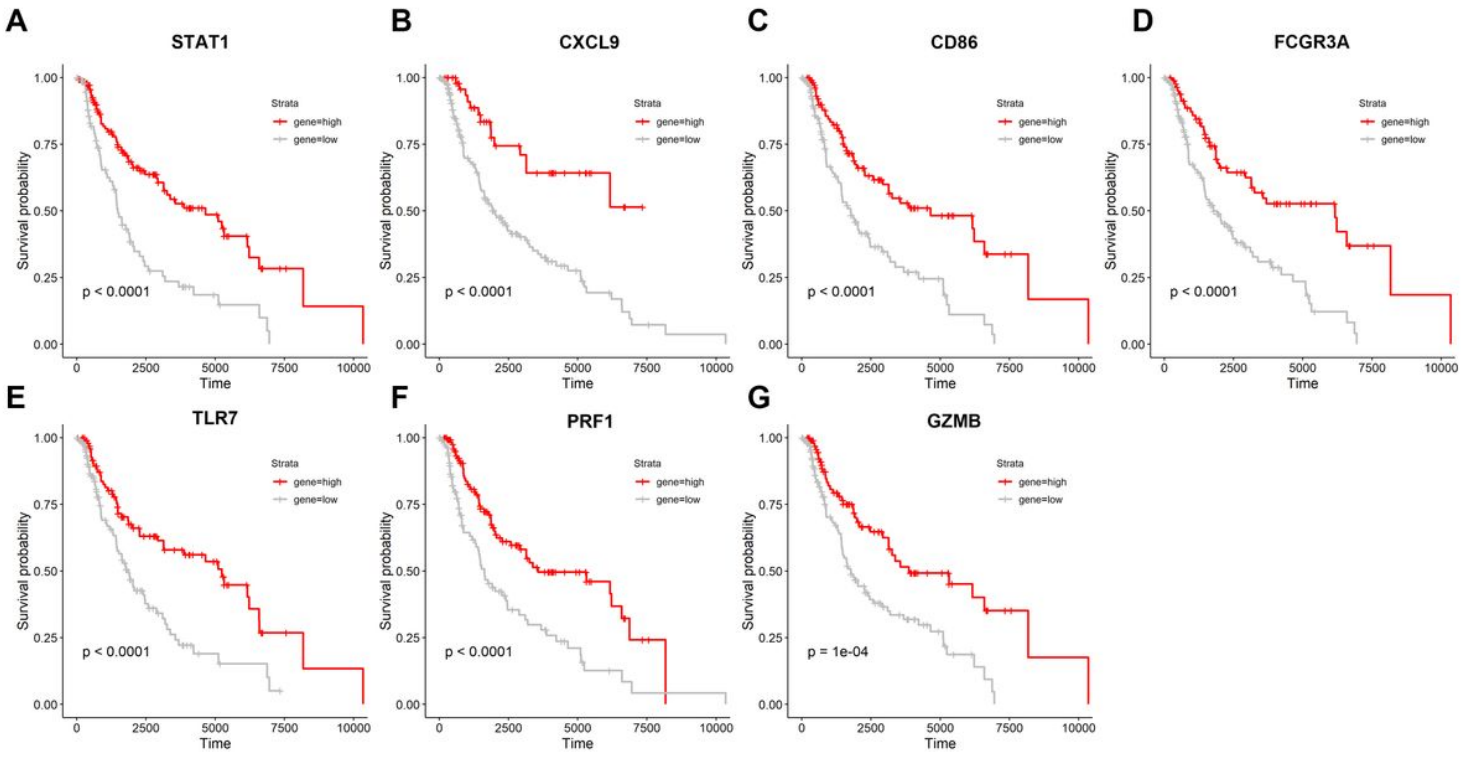

Figure 5

Survival analysis for seven key molecules. (A-G) Seven key molecules which includes STAT1, CXCL9, CD86, FCGR3A, TLR7, PRF1, GZMB.

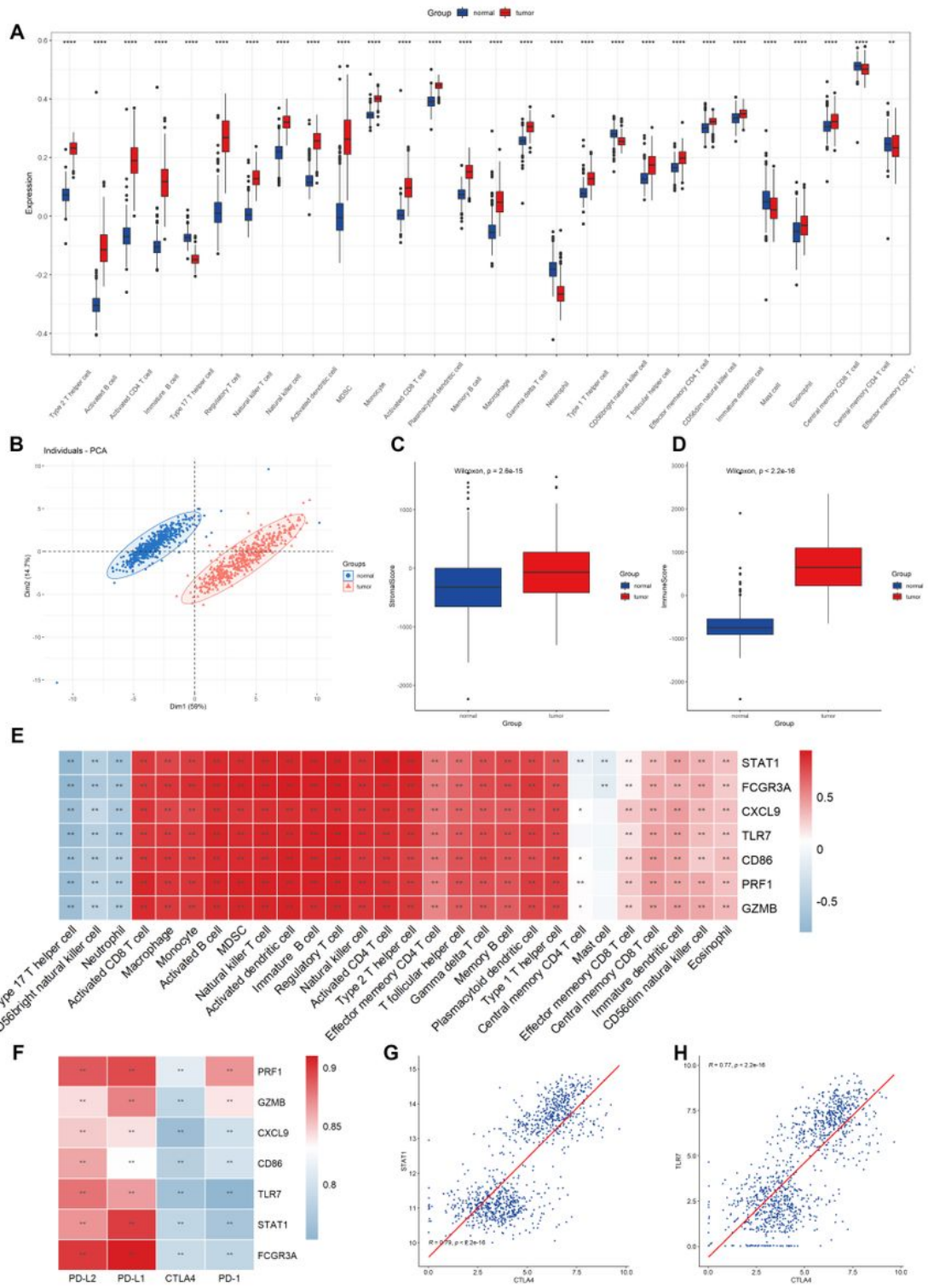

Figure 6

Evaluation of 28 TME immune cell infiltration characterization. (A) Differences in 28 TME infiltration cells between normal skin and skin cutaneous melanoma (*P<0.05, **P<0.01, ***P<0.001, ****P<0.0001). The results showed that all immune cells were significantly different between the two types of samples. (B) Principal component analysis. The results demonstrated that the two separate taxa, suggesting there existed significantly differences in the landscape of 28 TME immune cell infiltration between normal skin

and skin cutaneous melanoma. (C) Difference in StromalScore between normal and tumor tissues using ESTIMATE algorithm. (D) Difference in ImmuneScore between normal and tumor tissues using ESTIMATE algorithm. (E) The correlation between seven key molecule and each TME infiltration cell type. The results showed a strong correlation between them, red represents positive and blue represents negative. (F) The correlation between the seven key molecules and four immune checkpoint molecules. The results demonstrated a strong correlation between them. (G) The correlation between STAT1 expression and CTLA4 expression. (H) The correlation between TLR7 expression and CTLA4 expression.

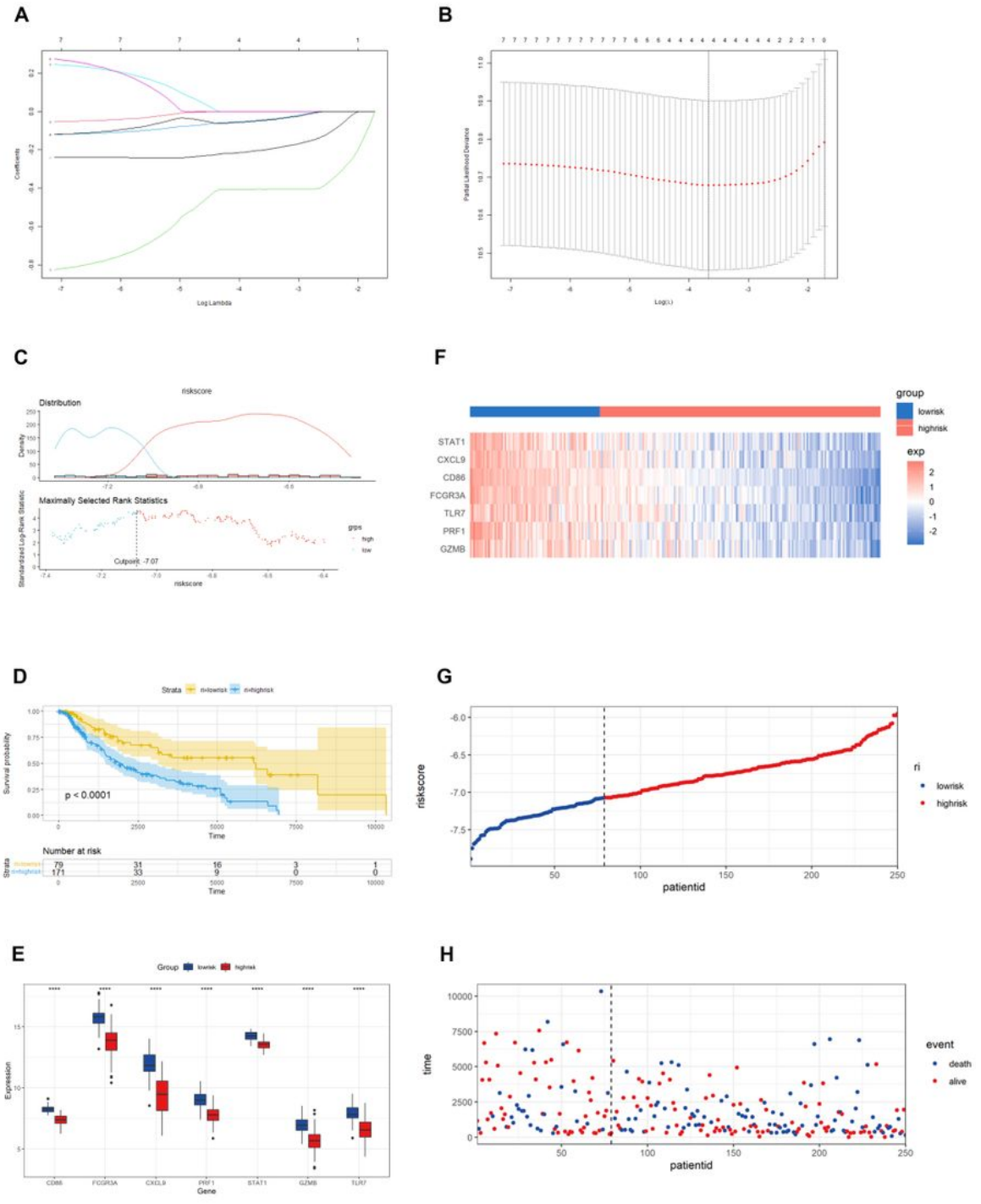

Figure 7

Construction of riskScore signature in skin cutaneous melanoma. (A) Least absolute shrinkage and selection operator (LASSO) coefficient profiles of the seven key molecules. Horizontal axis represents log of independent variable λ. Vertical axis represents coefficient of independent variable. (B) Tenfold cross-validation of tuning parameters in LASSO model. (C) The optimal cut-off point to dichotomize riskScore into low and high groups was determined by MaxStat R package. The optimal cutoff point was -7.07. (D) Survival analyses for low (79 samples) and high (171 samples) riskScore groups using Kaplan-Meier curves. (E) The seven key molecules expressed in the low and high risk groups (*P<0.05, **P <0.01, ***P <0.001, ****P <0.0001). The results showed that a strongly significant difference was exhibited between the groups. (F) The median value and distribution of the risk score. (G) The distribution of overall survival (OS) status. (H) Hierarchical clustering of seven key genes between low and high risk groups. Red represents up-regulated and blue represents down-regulated.

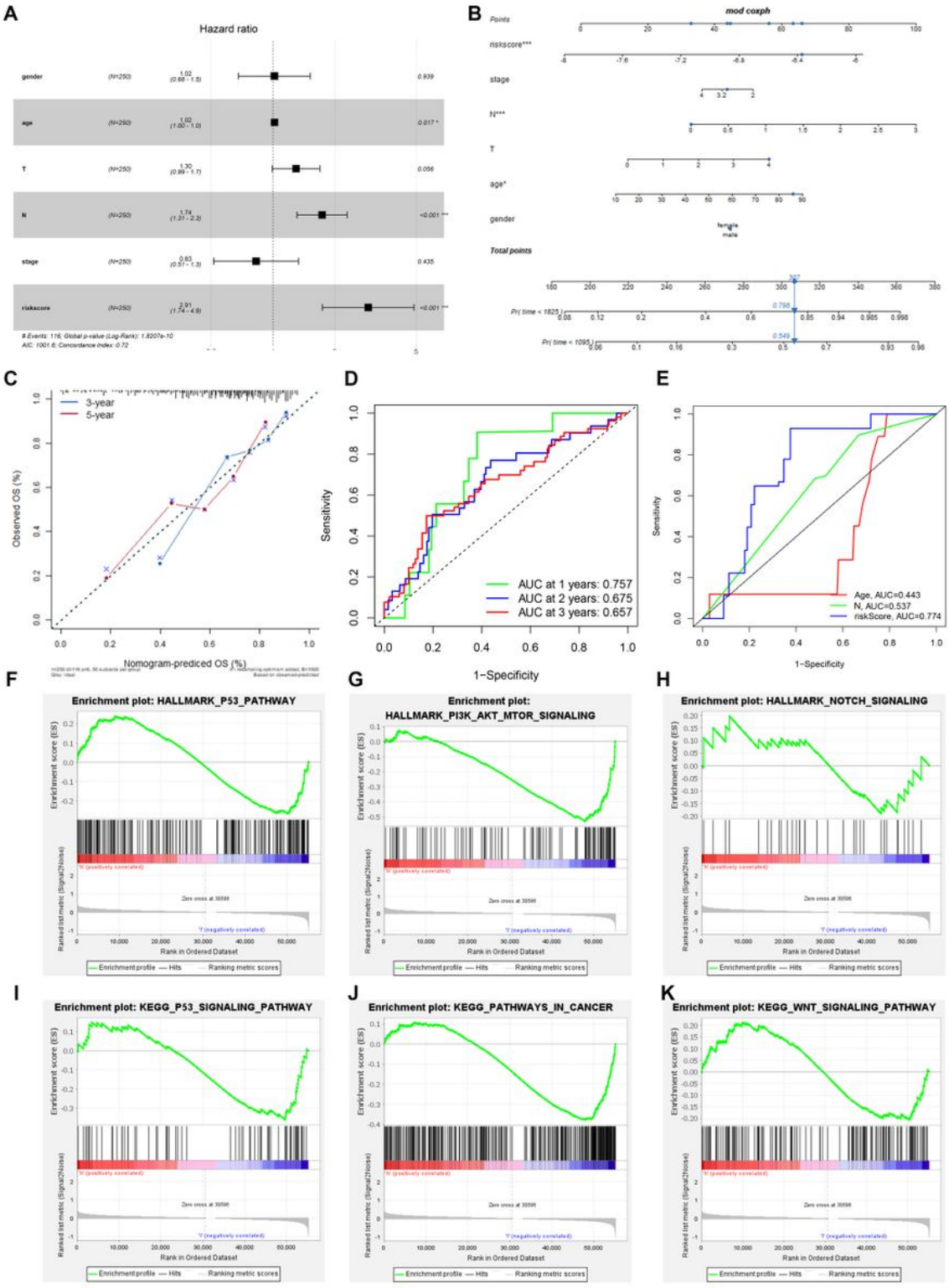

Figure 8

Prognostic value of the riskScore gene signature in skin cutaneous melanoma. (A) Forest plot. The results demonstrated that the riskScore and N were independent prognostic biomarkers using multivariate analyses. (B) The nomogram, including clinical features and the risk score, for predicting outcomes in patients. (C) The calibration curve analysis showed that the actual and the predicted 1-, 3-, 5-year survival times were consistent compared with the reference line (the 45-degree line). (D) The receiver operating

characteristic curve (ROC) analysis of risk scores based on 1-, 2-, and 3-year OS in TCGA group. (E) The receiver operating characteristic curve (ROC) analysis of risk scores and other clinical characteristics based on OS in TCGA group. (F-K) The GSEA enrichment reveal several significant signaling pathways. (F) HALLMARK P53 pathway. (G) HALLMARK PI3K AKT MTOR signaling pathway. (H) HALLMARK NOTCH signaling pathway. (I) KEGG P53 pathway. (J) KEGG pathway in cancer. (L) KEGG WNT signaling pathway.

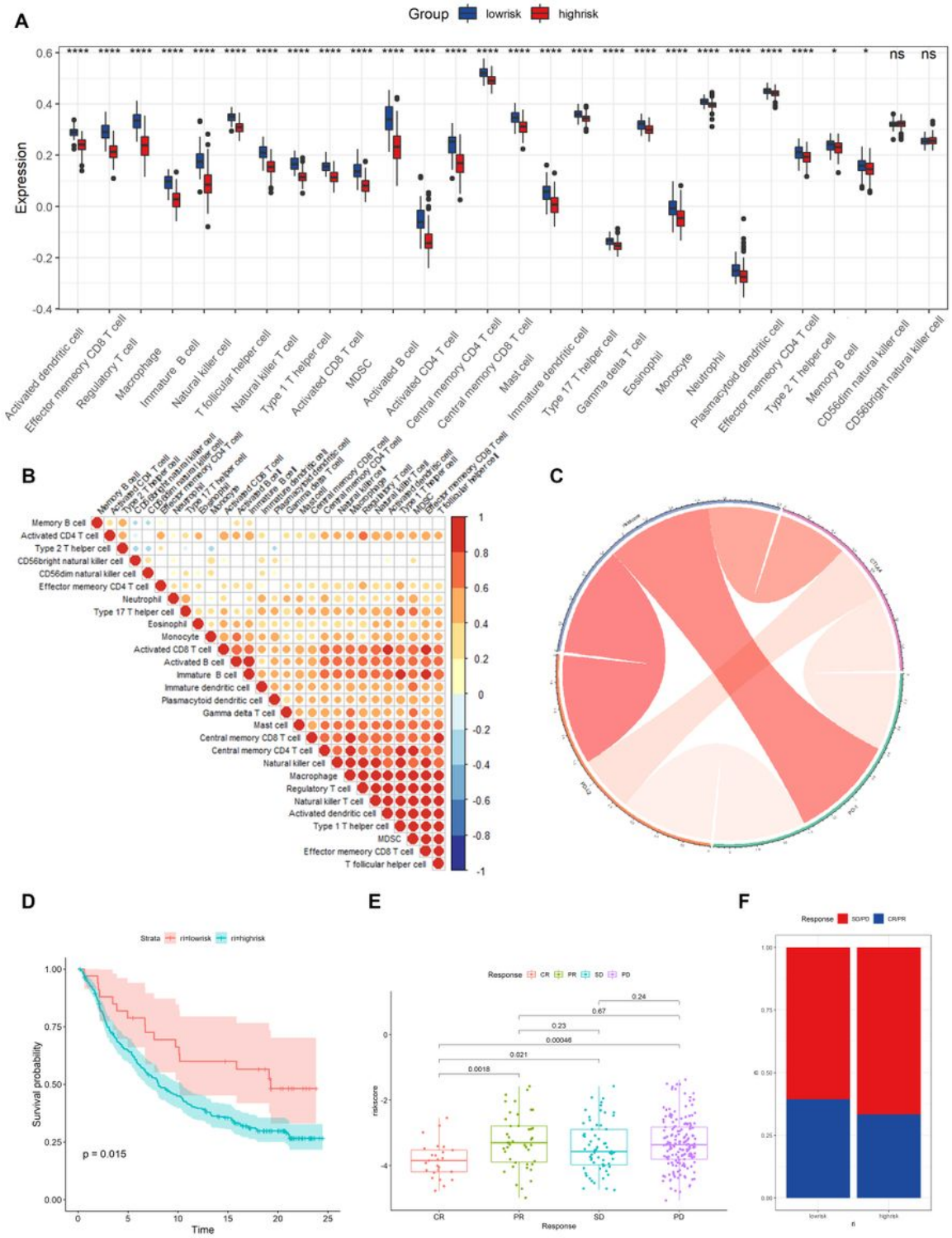

Figure 9

The role of riskScore signature in the TME cell infiltration and immunotherapeutic responses. (A) Differences in 28 TME infiltration cells between low and high risk groups (*P<0.05, **P <0.01, ***P <0.001, ****P <0.0001). The results demonstrated that most TME cells (26 types) exist significant differences. (B) The correlation between riskScore signature and 28 TME cell infiltration. Color shades represent the strength of the association, blue represents negative correlation and red represents positive correlation. (C) The correlation between riskScore signature and immune checkpoint molecules. Blue represents negative correlation and red represents positive correlation. (D) Survival analyses for high and lowriskScore groups in anti-PD-L1 immunotherapy cohort using Kaplan-Meier curves. (E) The difference of riskScore in different anti-PD-L1 clinical response groups. CR, complete response. PD, progressive disease. PR, partial response. SD, stable disease. (F) The proportion of patients with response to PD-L1 blockade therapy in high or low riskScore groups.

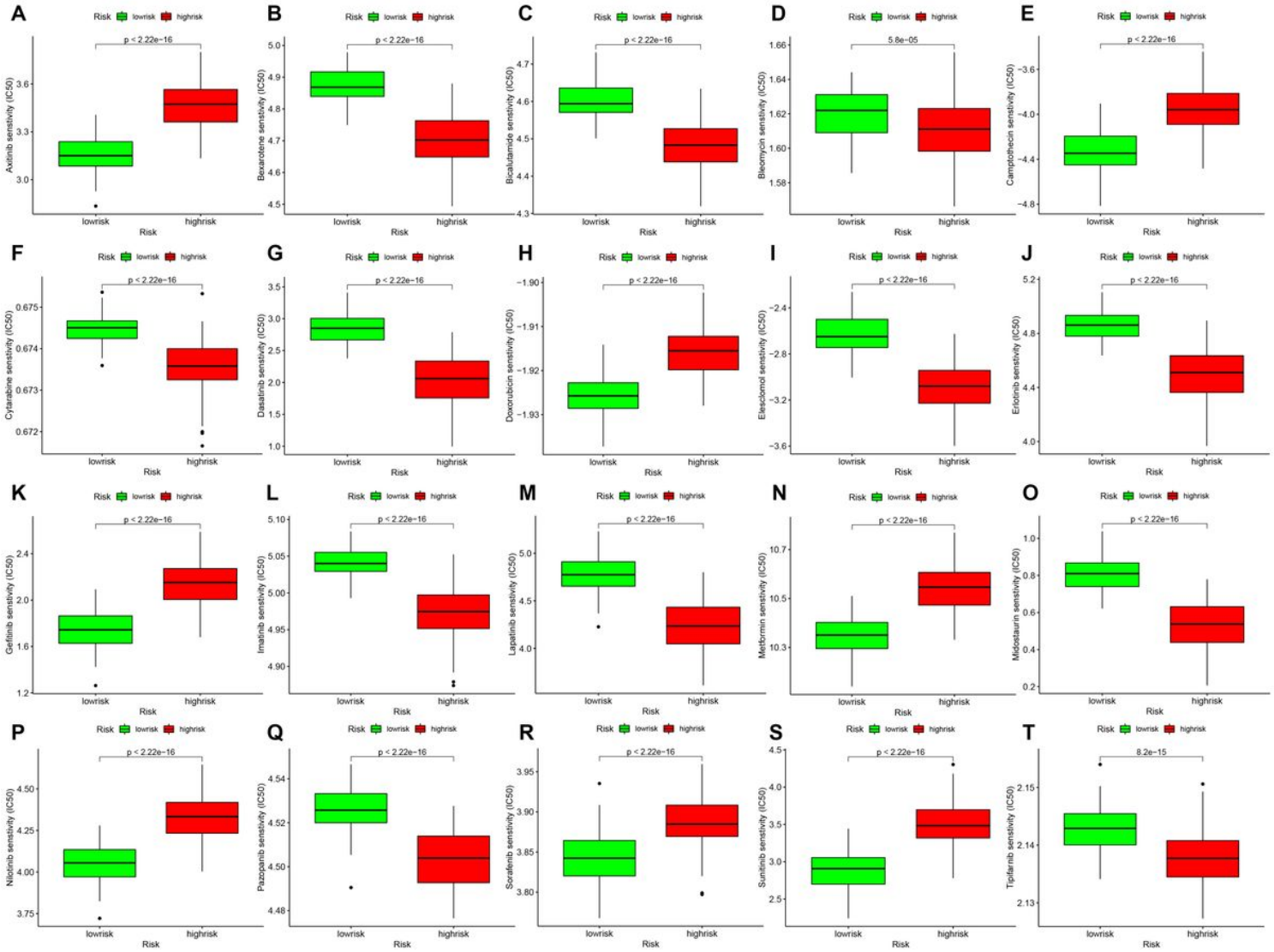

Figure 10

The riskScore signature is associated with chemotherapy and targeted therapy sensitivity. (A) Axitinib. (B) Bexarotene. (C) Bicalutamide. (D) Bleomycin. (E) Camptothecin. (F) Cytarabine. (G) Dasatinib. (H) Doxorubicin. (I) Elesclomol. (J) Erlotinib. (K) Gefitinib. (L) Imatinib. (M) Lapatinib. (N) Metformin. (O) Midostaurin. (P) Nilotinib. (Q) Pazopanib. (R) Sorafenib. (S) Sunitinib. (T) Tipifarnib.

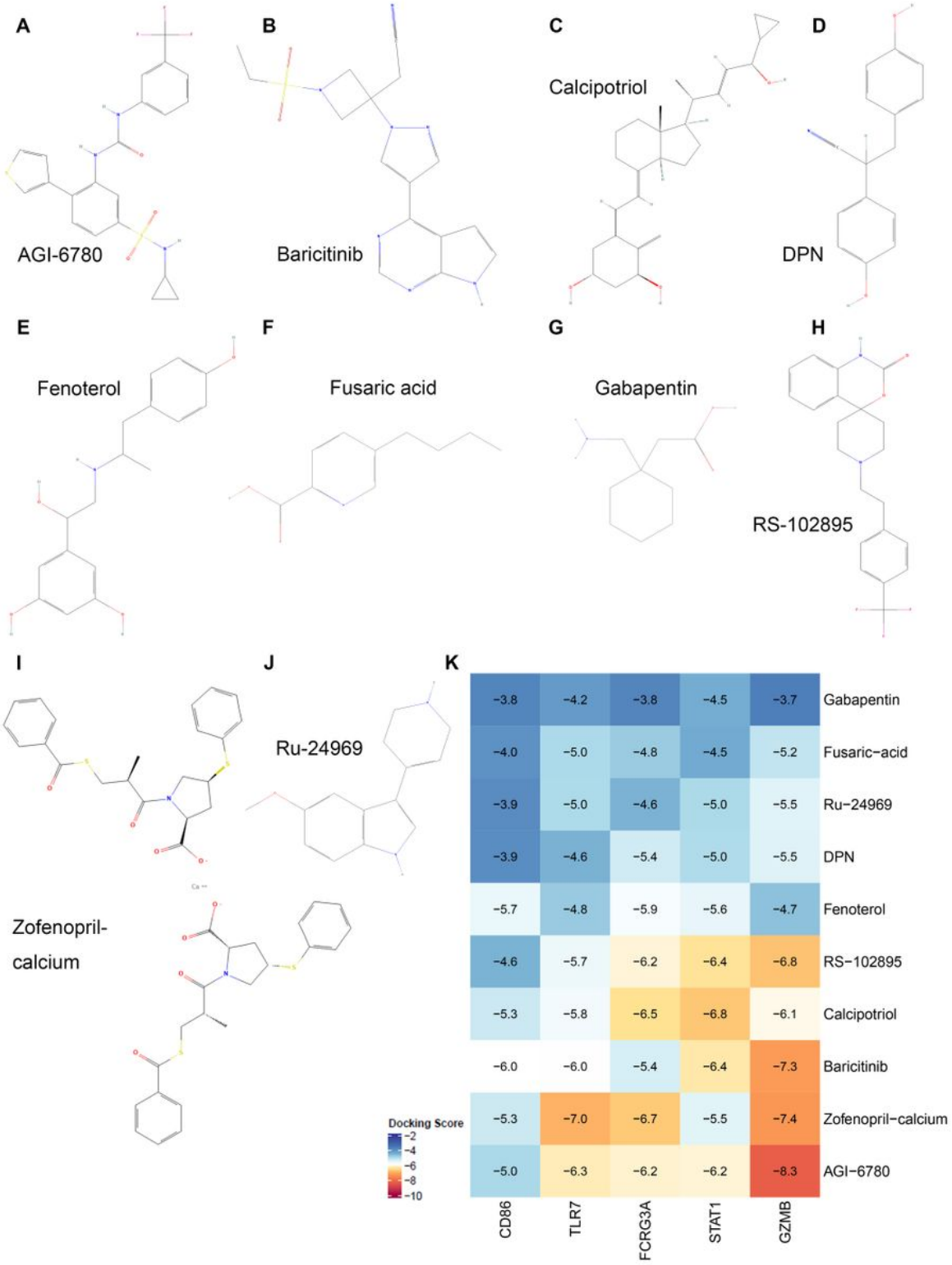

Figure 11

Chemical structure depiction of the top ten most significant drugs. (A) AGI-6780. (B) Baricitinib. (C) Calcipotriol. (D) DPN. (E) Fenoterol. (F) Fusaric acid. (G) Gabapentin. (H) RS-102895. (I) Zofenopril calcium. (J) Ru-24969. (K) Heat map of the lowest binding energy for molecular docking.

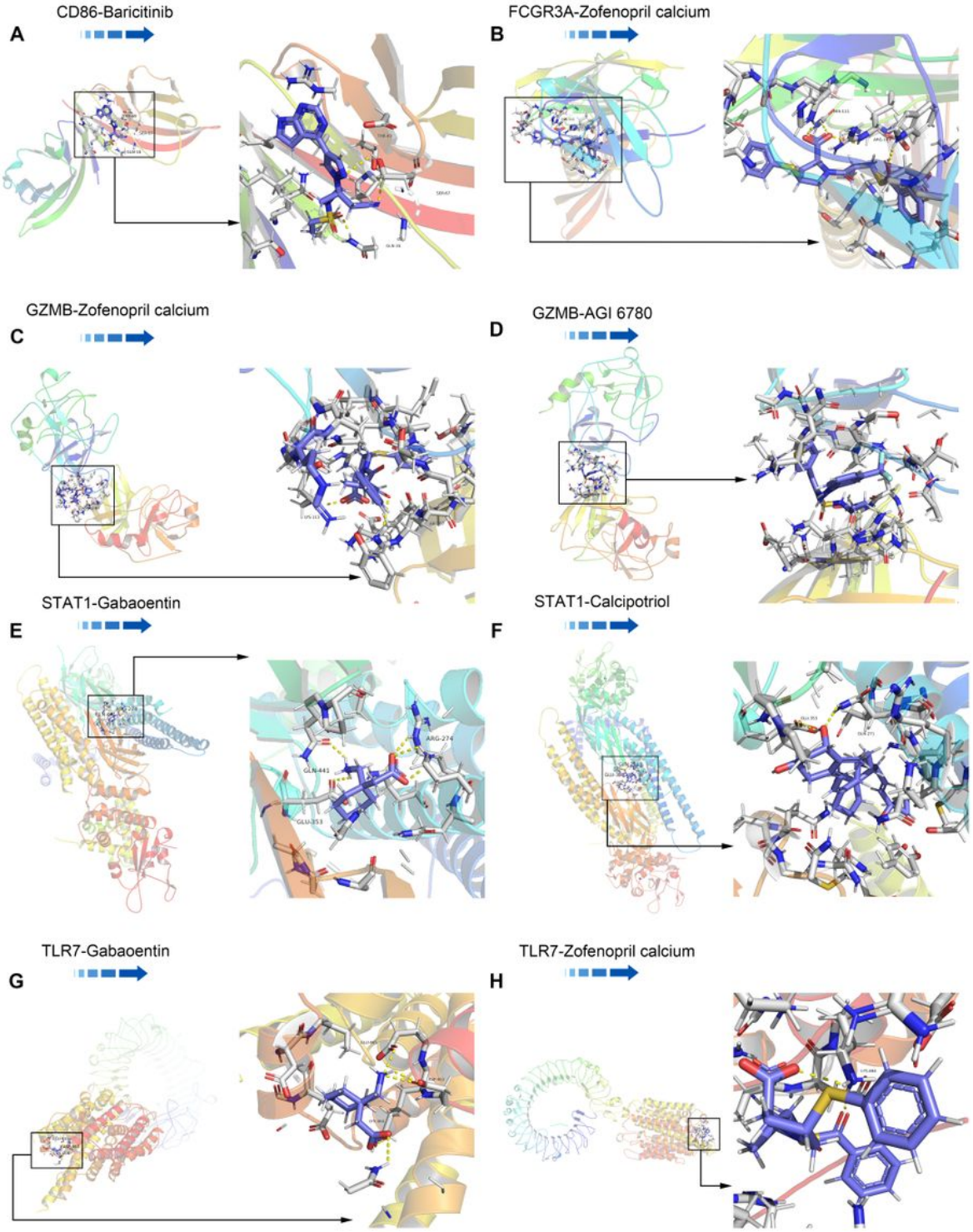

Figure 12

Docking diagram of small molecular drugs with targets. (A) CD86-Baricitinib. (B) FCGR3A-Zofenopril calcium. (C) GZMB-Zofenopril calcium. (D) GZMB-AGI 6780. (E) STAT1-Gabaoentin. (F) TLR7-Gabaoentin. (G) STAT1-Calcipotriol. (H) TLR7-Zofenopril calcium.

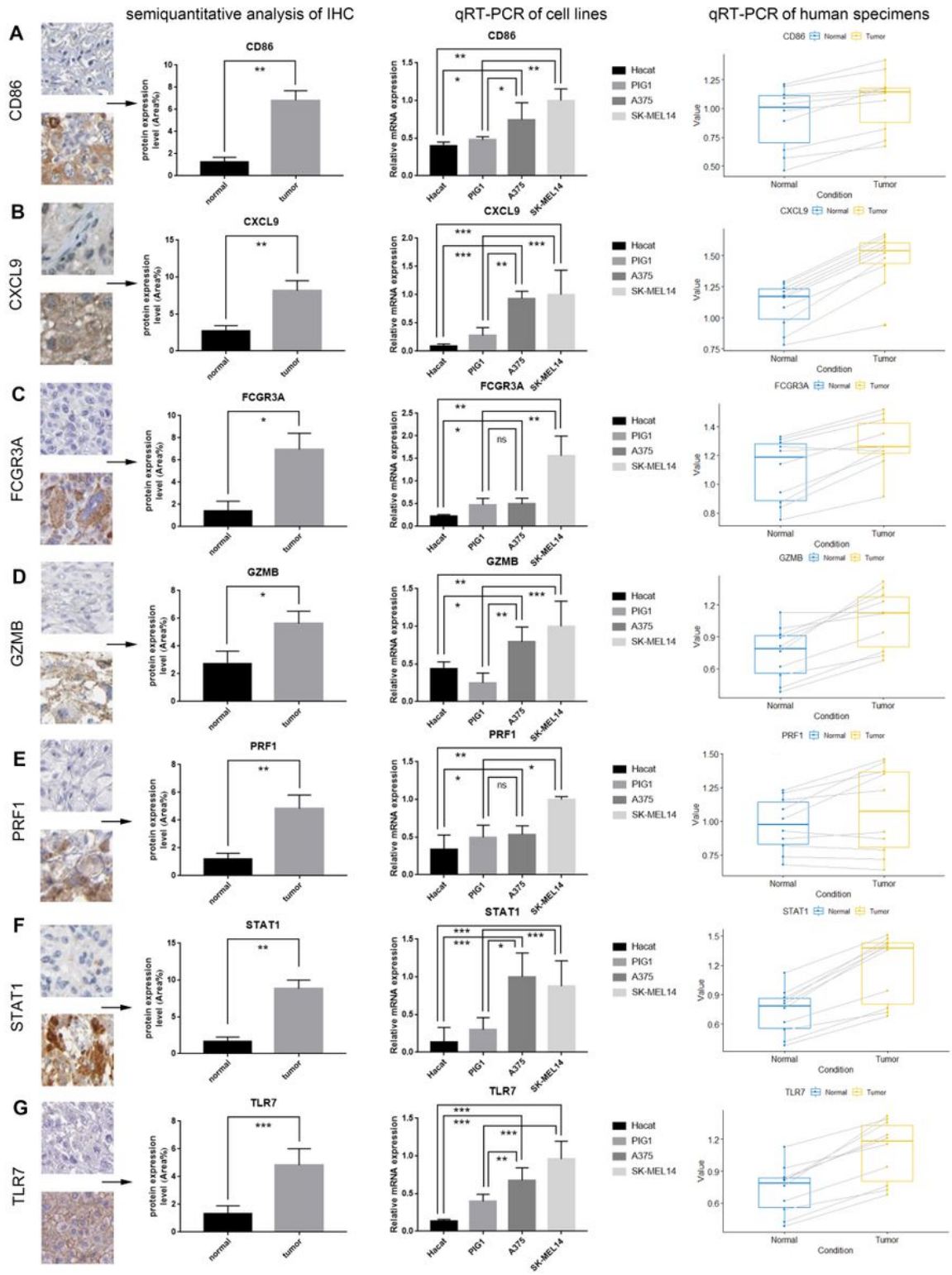

Figure 13

Validation of the mRNA and protein expression of seven key genes. Results of the first column represents the semiquantitative analysis results which obtained from the IHC results downloaded from the human protein atlas (see Figure 4 for a complete view of the immunohistochemistry images). Results of the second column represents the qRT-PCR results from four cell lines (Hacat, PIG1, A375 and SK-MEL 14). Results of the third column represents the qRT-PCR results of tissue specimens from 10 patients, which taken from normal skin and skin cutaneous melanoma. (A-G) represents the results of seven key genes, including CD86, CXCL9, FCGR3A, GZMB, PRF1, STAT1, TLR7 (ns, not significant, *P<0.05, **P <0.01, ***P <0.001).

Supplementary Files

This is a list of supplementary files associated with this preprint. Click to download.

- SupplementaryTable.docx